

AD-A100 728

USADAC TECHNICAL LIBRARY



5 0712 01015763 3

TECHNICAL
LIBRARY

AD

AD-E432 024

TECHNICAL REPORT ARLCD-TR-81006

MEASUREMENT OF PRESSURE AND RELATED ENERGY OUTPUT
FROM THERMALLY IGNITED PYROTECHNIC COMPOSITIONS
BURNING IN A PARTIALLY VENTED VESSEL

PATRICIA L. FARNELL
LEROY HUNTER
FRANCIS R. TAYLOR

MAY 1981



US ARMY ARMAMENT RESEARCH AND DEVELOPMENT COMMAND
LARGE CALIBER
WEAPON SYSTEMS LABORATORY
DOVER, NEW JERSEY

APPROVED FOR PUBLIC RELEASE: DISTRIBUTION UNLIMITED

The views, opinions, and/or findings contained in this report are those of the author(s) and should not be construed as an official Department of the Army position, policy or decision, unless so designated by other documentation.

Destroy this report when no longer needed. Do not return it to the originator.

UNCLASSIFIED

SECURITY CLASSIFICATION OF THIS PAGE (When Data Entered)

20. ABSTRACT (cont)

These experiments showed that the pressure increased linearly with (a) increasing loading density for a constant vent, and (b) decreasing vent size for constant loading density. For the linear part of the pressure-time trace, dP/dt also increased with increasing loading density and with decreasing vent size. This latter result shows the effect of pressure on burning rate.

Velocities of the air pressure wave were obtained in excess of the speed of sound, indicating a low velocity detonation had taken place. Very low TNT equivalences for pressure were obtained, the largest being only 0.61; those for impulse were 0.6 through 0.9 with the smallest vent for the compositions (except the gasless delay powder which was only 0.05), reflecting the relatively long duration of positive pressure produced by these compositions.

SUMMARY

In an effort to determine the hazards of preparing pyrotechnic compositions in processing bays, a study was conducted in which a series of compositions were thermally ignited in a vented vessel and the resulting pressure versus time, rate of pressure rise (dP/dt), and velocity of the air pressure wave were measured. The compositions were a standard illuminating material, a photoflash powder, an igniter, a delay powder, and a formulation which generates infrared (IR) radiation.

These experiments showed that the pressure increased linearly with (a) increasing loading density for a constant vent, and (b) decreasing vent size for constant loading density. For the linear part of the pressure-time trace, dP/dt also increased with increasing loading density and with decreasing vent size. This latter result shows the effect of pressure on burning rate.

Velocities of the air pressure wave were obtained in excess of the speed of sound, indicating a low velocity detonation had taken place. Very low TNT equivalences for pressure were obtained, the largest being only 0.16; those for impulse were 0.6 through 0.9, with the smallest vent for the compositions (except the gasless delay powder which was only 0.05), reflecting the relatively long duration of positive pressure produced by these compositions.

CONTENTS

	Page
Introduction	1
Experimental Procedure	1
Results and Discussion	6
Pressure as a Function of Time Inside Vessel	6
Rate of Pressure Rise (dP/dt) Inside Vessel	20
Scaled Impulse Inside Vessel	20
Scaled Duration of Pressure Inside Vessel	36
Pressure Environment Outside the Vessel	42
TNT Equivalencies	47
Conclusions	49
References	51
Appendix	53
List of Symbols	61
Distribution List	63

TABLES

	Page
1 Dimensions for pressure vessel	4
2 Formulation of compositions	6
3 Compositions producing supersonic pressure wave	47
4 TNT equivalencies for pressure	48
5 TNT equivalencies for impulse	48

FIGURES

	Page
1 Cross sectional view test vessel	2
2 Experimental setup with vessel in box and detectors in metal plate	3
3 Sample oscillographic trace showing ignition pulse and the output from detectors 1 to 5	5
4 Graphs of pressure versus loading density for low values of PFP-555	7
5 Graphs of pressure versus loading density for high values of PFP-555	8
6 Graphs of pressure versus loading density for SI-193	9
7 Graphs of pressure versus loading density for FW-306	10
8 Graphs of pressure versus loading density for PFP-555	11
9 Graphs of pressure versus loading density for FY-1451	12
10 Graphs of pressure versus loading density for DP-973	13
11 Graphs of pressure versus venting for SI-193	15
12 Graphs of pressure versus venting for FW-306	16
13 Graphs of pressure versus venting for PFP-555	17
14 Graphs of pressure versus venting for FY-1451	18
15 Graphs of pressure versus venting for DP-973	19
16 Graphs of dP/dt versus loading density for SI-193	21
17 Graphs of dP/dt versus loading density for FW-306	22
18 Graphs of dP/dt versus loading density for PFP-555	23
19 Graphs of dP/dt versus loading density for FY-1451	24
20 Graphs of dP/dt versus loading density for DP-973	25

21	Graphs of dP/dt versus venting for SI-193	26
22	Graphs of dP/dt versus venting for FW-306	27
23	Graphs of dP/dt versus venting for PFP-555	28
24	Graphs of dP/dt versus venting for FY-1451	29
25	Graphs of dP/dt versus venting for DP-973	30
26	Graphs of scaled impulse versus scaled vent area for SI-193	31
27	Graphs of scaled impulse versus scaled vent area for FW-306	32
28	Graphs of scaled impulse versus scaled vent area for PFP-555	33
29	Graphs of scaled impulse versus scaled vent area for FY-1451	34
30	Graphs of scaled impulse versus scaled vent area for DP-973	35
31	Graphs of scaled duration of pressure versus scaled vent area for SI-193	37
32	Graphs of scaled duration of pressure versus scaled vent area for FW-306	38
33	Graphs of scaled duration of pressure versus scaled vent area for PFP-555	39
34	Graphs of scaled duration of pressure versus scaled vent area for FY-1451	40
35	Graphs of scaled duration of pressure versus scaled vent area for DP-973	41
36	Graphs of pressure outside vessel versus loading density for SI-193	43
37	Graphs of pressure outside vessel versus loading density for FW-306	44

38 Graphs of pressure outside vessel versus
loading density for PFP-555 45

39 Graphs of pressure outside vessel versus
loading density for FY-1451 46

INTRODUCTION

A great deal of work has been performed to determine the effect on facilities and personnel of detonation of high explosives in confined areas, such as a processing room or a storage bunker (refs 1,2). However, few studies have been made on the hazards of accidental ignition of pyrotechnic compositions to these facilities and personnel. It has been found that ignition of a pyrotechnic composition by a detonation can, in some cases, cause the material itself to detonate (refs 3,4). It is also known that it is possible to cause these compositions to detonate upon ignition by a thermal source such as a squib or electric match when completely confined in a zero ullage system (ref 5). The study described in this report was undertaken to determine the pressure buildup and impulse imparted to the walls of the confined space, and to determine if the burning can become a detonation, when the compositions are ignited thermally in a vessel with various sized vents in the lid of the vessel, and when the composition occupies only a small portion of the volume of the vessel.

EXPERIMENTAL PROCEDURE

The test container consisted of a cylindrical, high pressure vessel with inside dimensions of 7.6 cm (3 in.) diameter by 30.5 cm (12 in.) long, and with 1.9 cm (3/4 in.) thick stainless steel walls. The vessel was fitted with two tapped openings (A and C on fig. 1) for pressure transducers and an opening for a conax fitting. Stainless steel plates 1.3 cm (1/2 in.) thick with various vent sizes were held tightly against the end of the vessel by four 0.6 cm (1/4 in.) by 5.0 (2 in.) brass bolts through a retaining ring welded to the vessel, with the plate seated on an "O" ring seal.

The cylindrical vessel was held in horizontal position by mounting it in a wooden box 25 x 61 x 40 cm (10 in. x 24 in. by 16 in.) (fig. 2). The box was seated on a large table on top of which was a 0.6 cm thick aluminum plate containing holes for mounting pressure transducers flush with the top of the plate. The dimensions of the vessel and the vent sizes are listed in table 1. In later experiments transducer no. 5 was mounted 366 cm (12 ft) from the vessel facing the vent directly (not shown on fig. 2).

The compositions were placed in a thin plastic bag, made spherical in shape, with a squib embedded in the composition. The bag was taped to a small piece of asbestos, which minimized burning of the surface of the vessel, and the whole assembly pushed to the closed end of the vessel. The maximum size of the composition was 6.4 cm (2.5 in.) diameter, with a volume less than 10% of the total inside

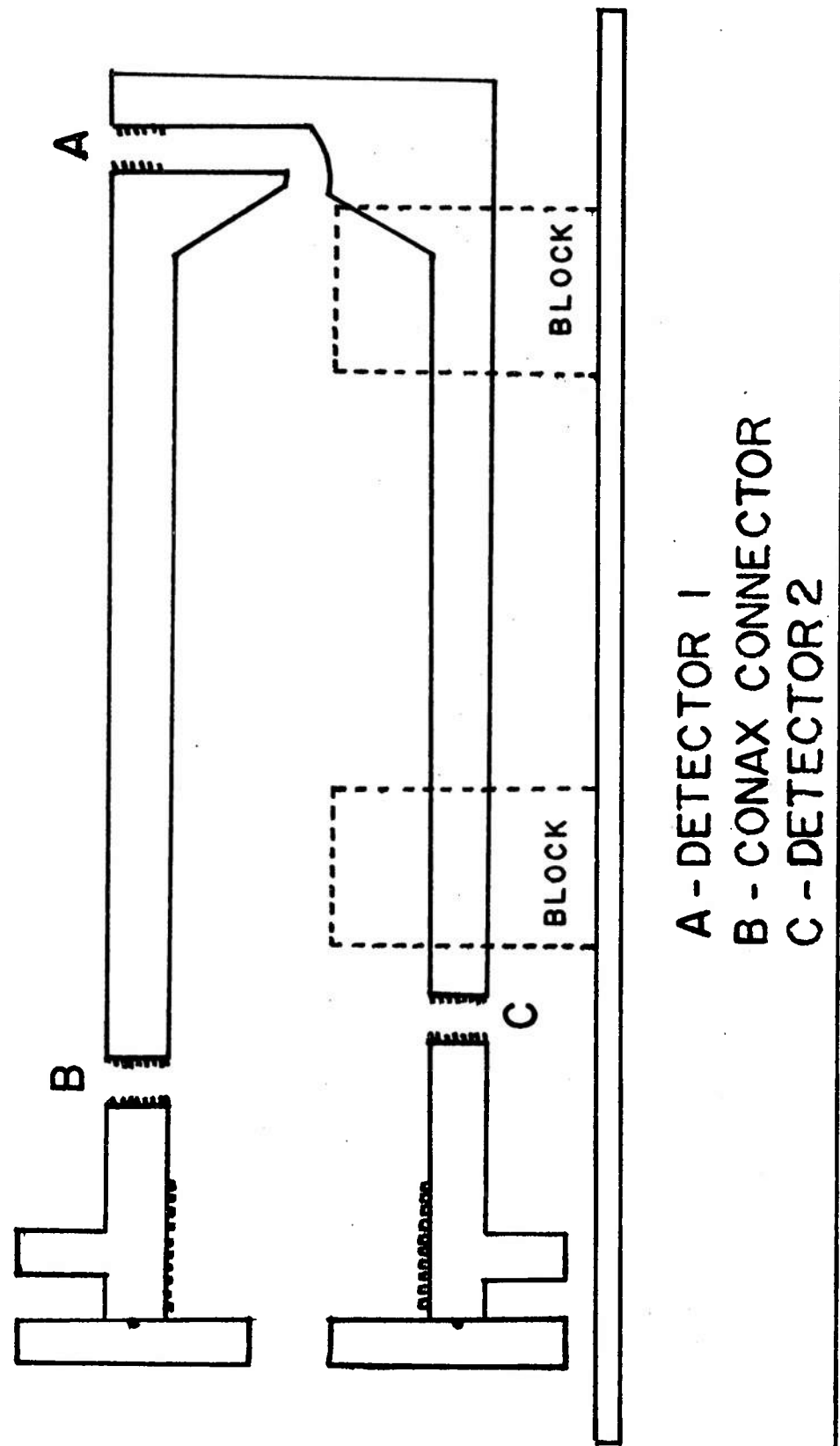


Figure 1. Cross sectional view test vessel

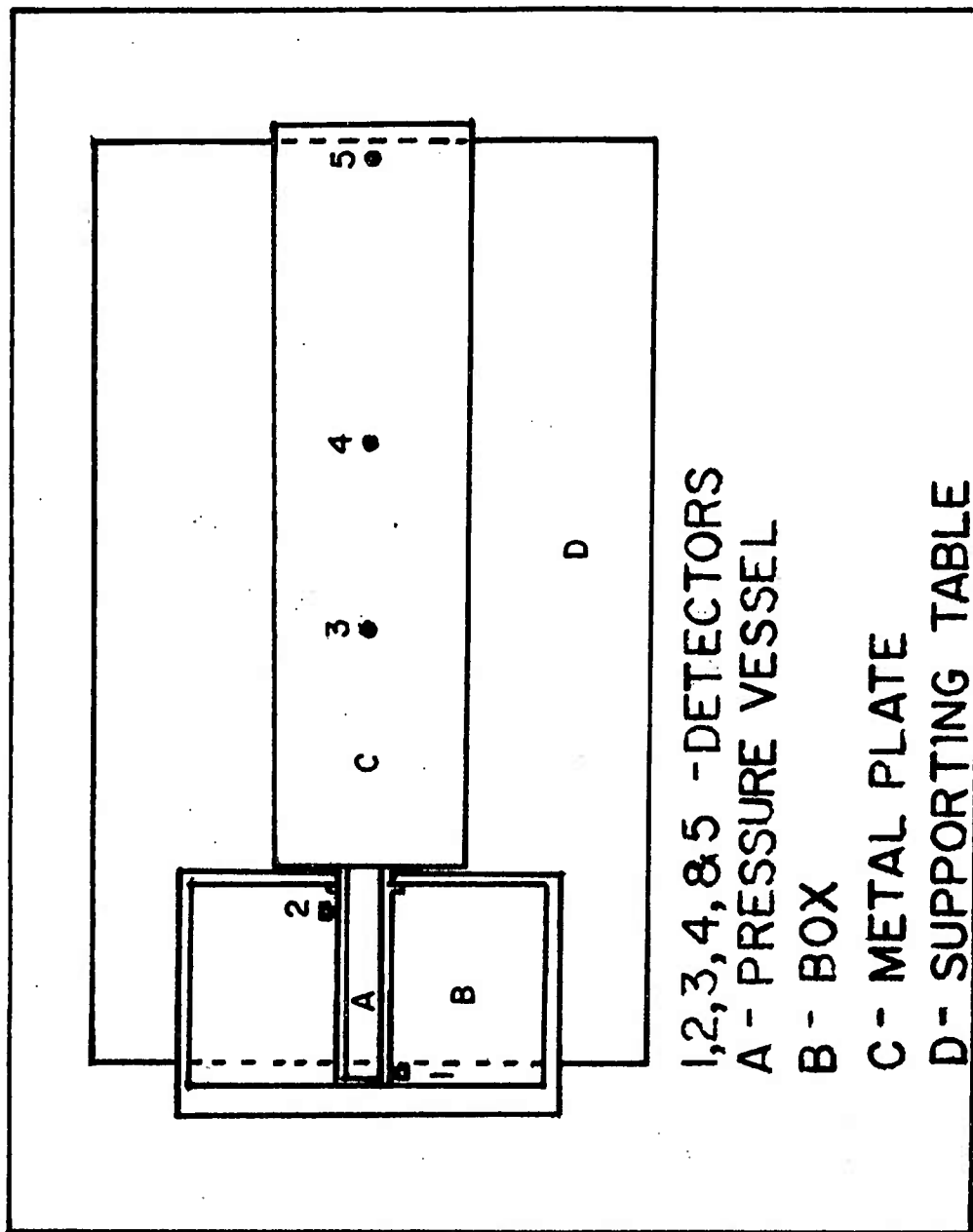


Figure 2. Experimental setup with vessel in box and detectors in metal plate

volume of the vessel. The electrical leads of the squib were fastened through the conax fitting to a 45 V battery circuit.

Table 1. Dimensions for pressure vessel

$$\text{Volume of vessel } V = 1500 \text{ cm}^3 (0.0550 \text{ ft}^3)$$
$$V^{2/3} = 131 \text{ cm}^2 (0.141 \text{ ft}^2)$$

Vent diameter cm	Vent area A cm ²	(in.)	(ft ²)
7.6	45.6	(3)	(0.0491)
5.0	20.3	(2)	(0.0218)
2.5	5.1	(1)	(0.00545)
1.9	2.9	(3/4)	(0.00307)
1.3	1.3	(1/2)	(0.00136)
0.6	0.3	(1/4)	(0.000341)

The detectors employed were Tyco strain gauge pressure transducers, activated by 5 V power supplies. These detectors were channeled through a DC amplifier to a Honeywell visicorder oscillograph, model 1508. A sample trace is shown in figure 3. The ignition pulse was supplied at the time that the ignition switch is thrown; the traces are all of voltage versus time.

The values measured were peak pressure, time from ignition to beginning of pressure rise, duration of positive pressure, and elapsed time from the beginning of pressure rise to peak pressure. Values calculated were dP/dt (rate of pressure rise on straight line part of trace), impulse, TNT equivalencies, and velocity of pressure wave.

Table 2 lists the compositions studied. These cover a wide range of types. FY-1451 is a standard illuminating composition; PFP-555 is a photoflash powder; FY-306 is an infrared composition; SI-193 is an igniter composition, and DP-973 is a delay powder. The system was calibrated by detonating C4 explosive with 7.6, 5.0 and 2.5 cm vents. Below 2.5 cm there was no change in pressure with changing vent size. The TNT equivalencies were calculated for pressure and impulse inside the vessel by dividing the value obtained for the composition by 0.80 times the value for C4 (0.8 converts C4 to TNT) times the ratio of wt of C4 to wt of composition.

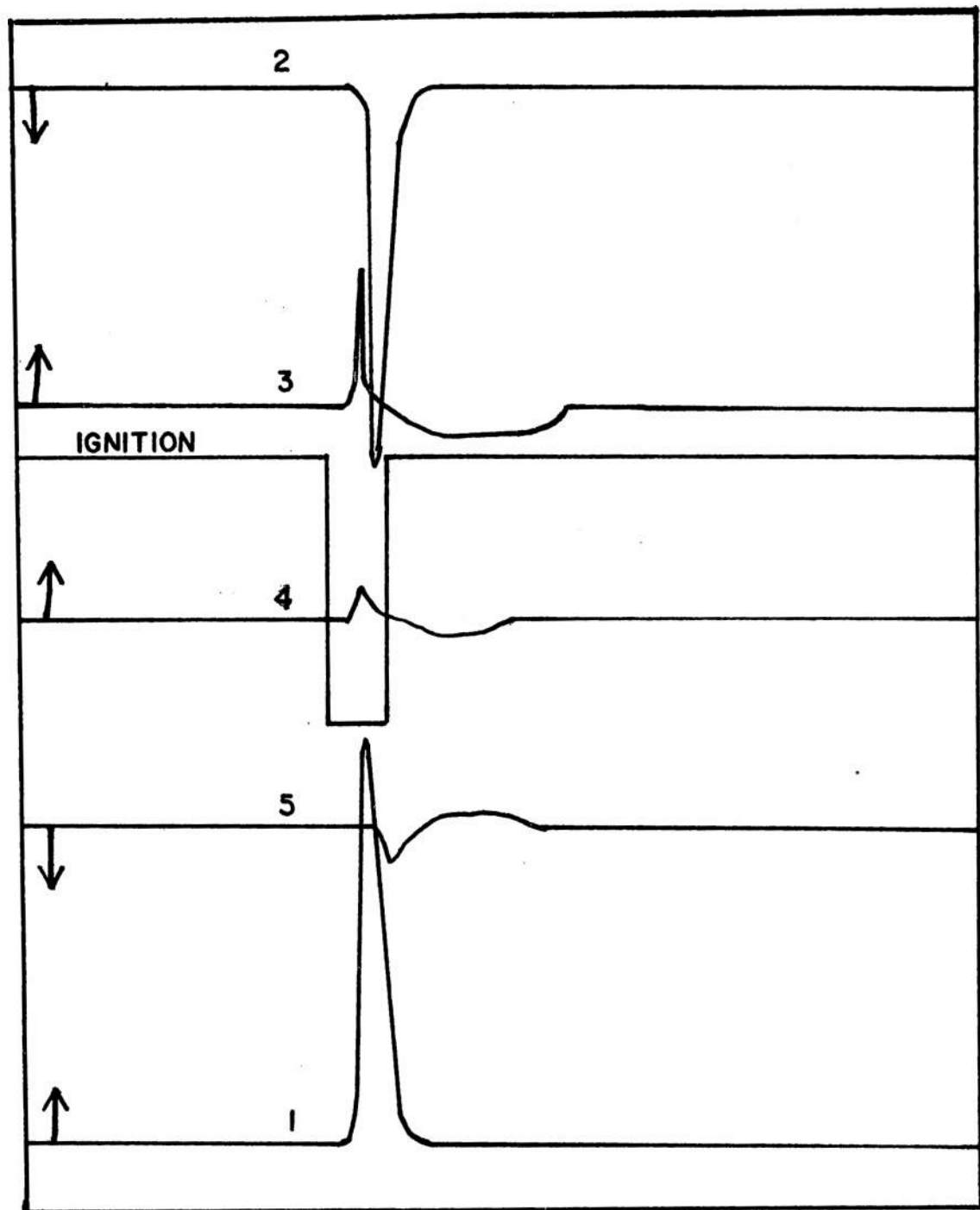


Figure 3. Sample oscillosgraphic trace showing ignition pulse and the output from detectors 1 to 5

Table 2. Formulation of compositions

Designation	Formulation
FY-1451	46% Mg - 45% NaNO ₃ - 9% laminac
PFP-555	40% Al - 30% Ba(NO ₃) ₂ - 30% KC1O ₄
FW-306	52.6% Mg - 44.8% Teflon - 2.6% nitrocellulose
SI-193	74% KNO ₃ - 25% B - 1% VAAR
DP-973	89% BaCrO ₄ - 10% B - 1% VAAR

RESULTS AND DISCUSSION

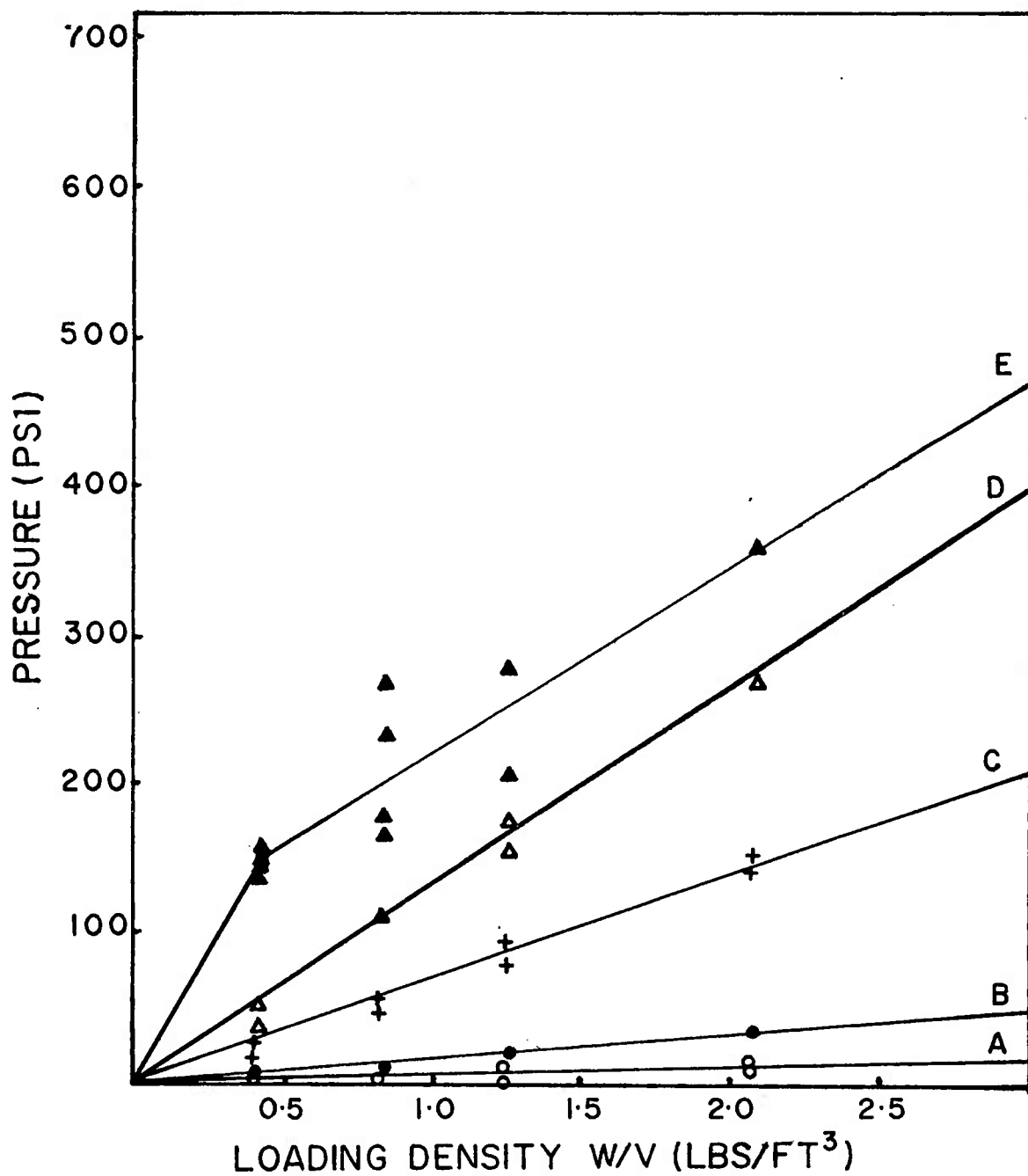
One unusual phenomenon became apparent upon examining the data from detector 1: For all compositions except DP-973, the values for pressure, dP/dt , and impulse tended to divide into a high group and a low group. Generally, the data indicated that pressure rose more rapidly in the high group, reached a higher value, and because the duration was about the same, yielded a higher impulse. Figure 4 shows plots of pressure versus W/V for the low values, while figure 5 shows those for the high values. It was not possible to predict which group a composition would fall into before it was ignited, and since the average of all values falls between the two groups, only average values were used for the rest of the curves.

The difference in the types of reactions involved were clearly demonstrated with small vents. For 1.25 cm (1/2 in.) and 0.6 cm (1/4 in.) vents, 50 g of SI-193 developed sufficient force to shear off the bolts holding the lid on the vessel. For PFP-555, 50 g caused this to occur only for the 0.6 cm vent, while only one of six trials for 50 g of FY-1451 with 0.6 cm vent developed enough force to shear off the bolts. In the case of FW-306, the extreme heat produced by the reaction melted a groove about 0.3 cm (1/8 in.) deep and 7.6 cm (3 in.) long in the top of the vessel; this relieved the pressure sufficiently to prevent shearing the bolts. The burning of DP-973 caused none of these occurrences, the vessel remaining intact for all sample weights and vent sizes.

Pressure as a Function of Time Inside Vessel

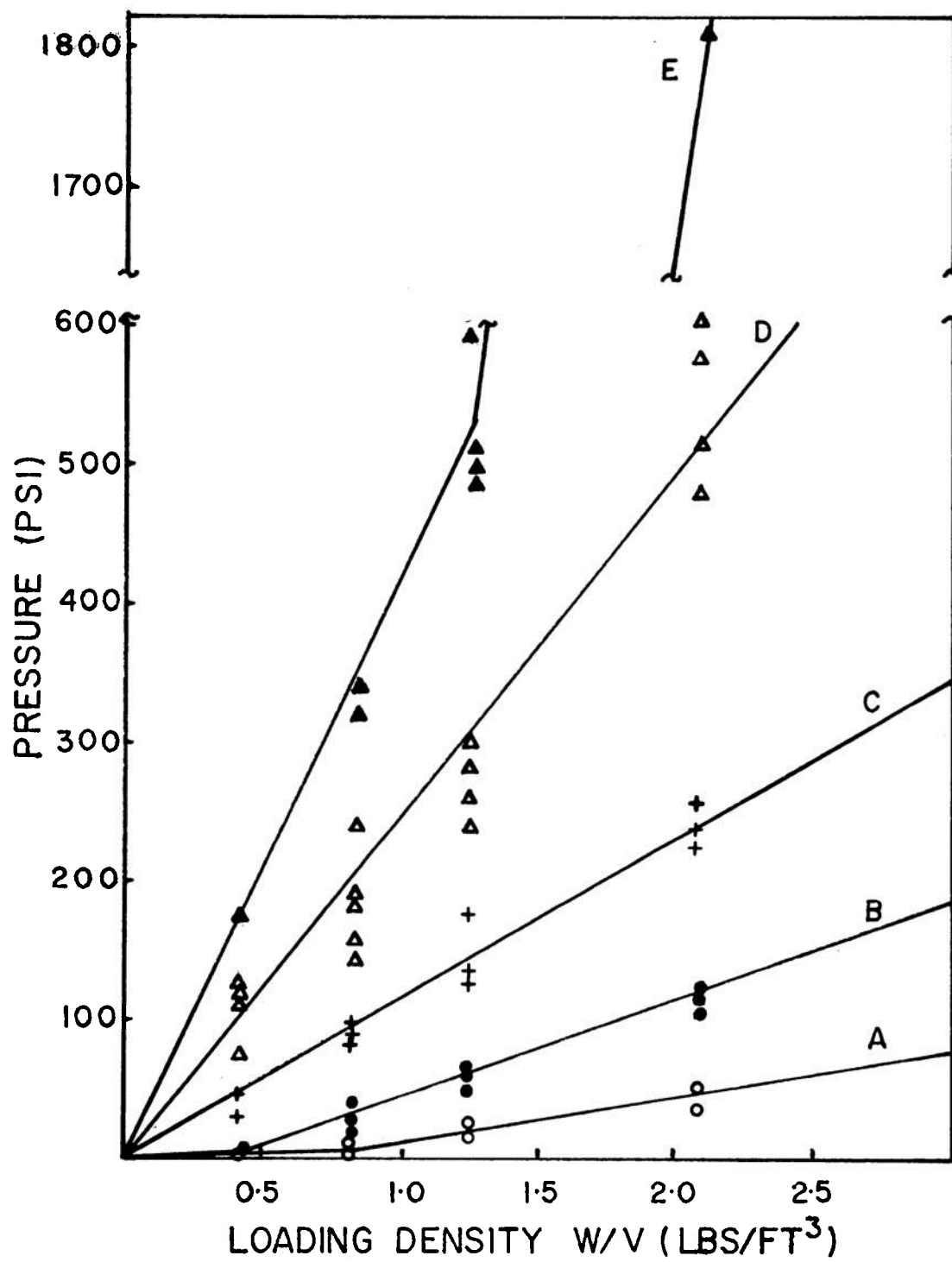
Figures 6 through 10 illustrate plots of p versus W/V for different vent sizes, for each composition. Figures 6, 7, 9, and 10 also show curves of peak pressure versus loading density using a nonvented or completely closed pressure vessel. Generally, the peak pressure show a linear dependence of W/V of the form

$$p = a W/V + b \quad (1)$$



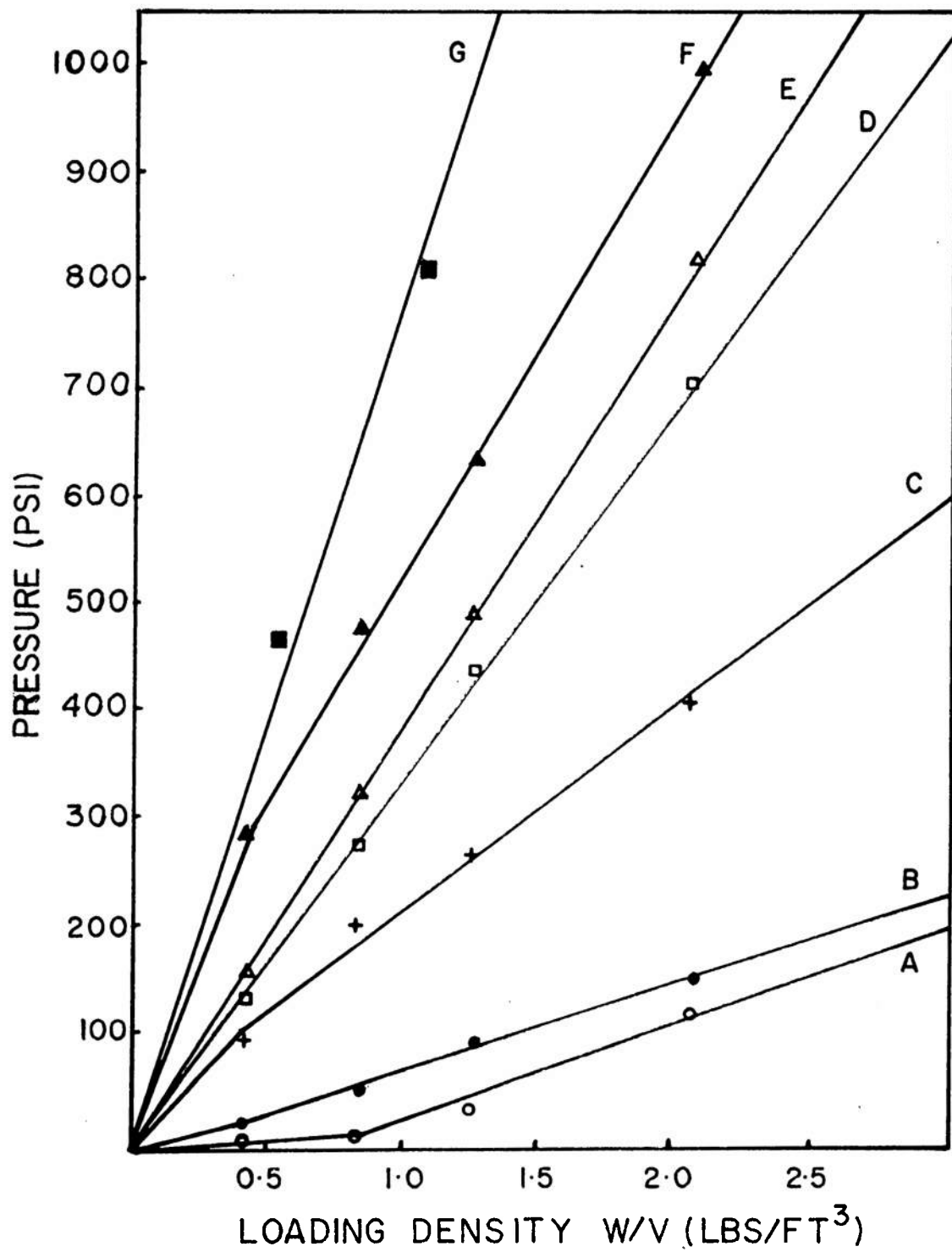
Note: Curves represent the following venting: a = 3 in., b = 2 in., c = 1 in., d = 1/2 in., e = 1/4 in.

Figure 4. Graphs of pressure versus loading density for low values of PFP-555



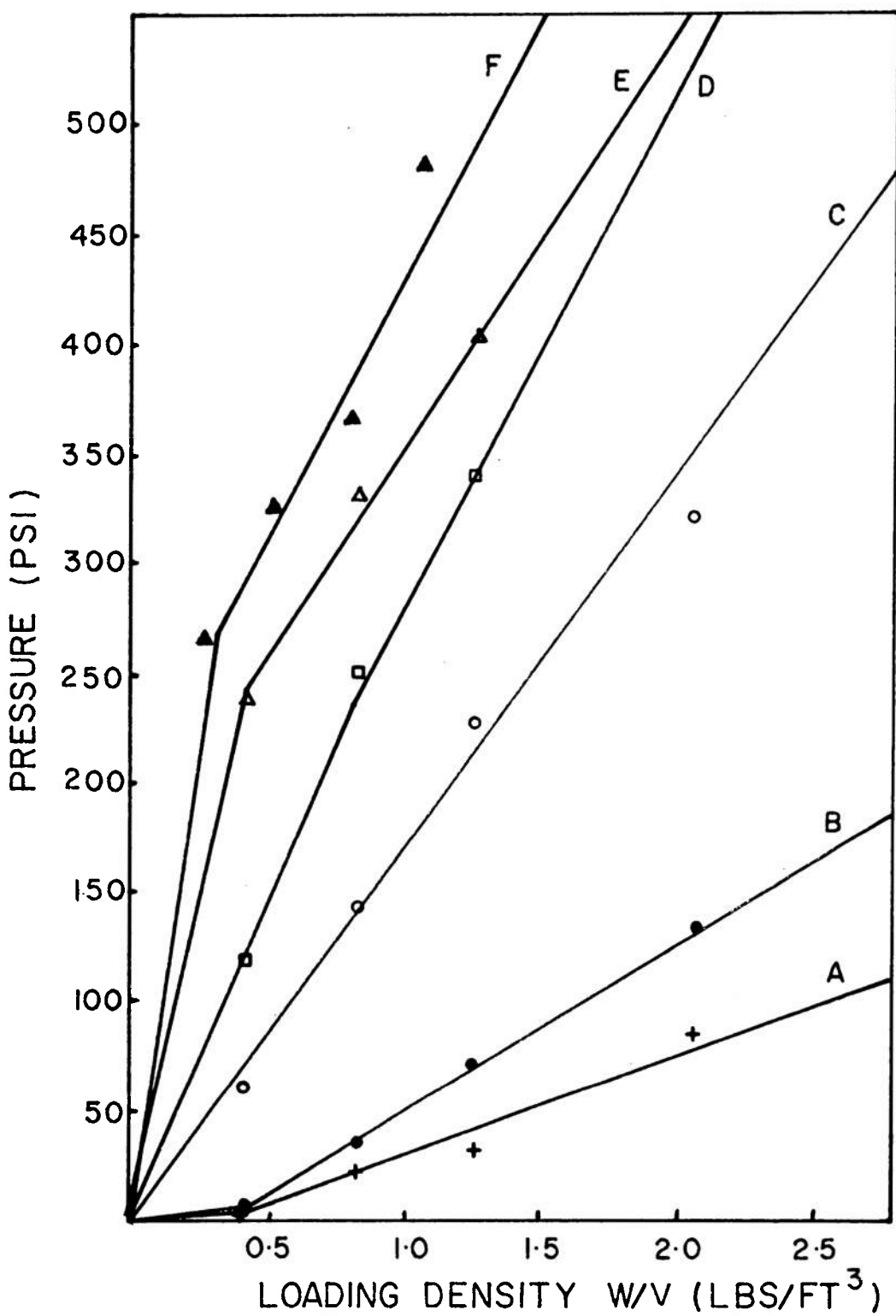
Note: Curves represent the following venting: a = 3 in., b = 2 in.,
 c = 1 in., d = 1/2 in., e = 1/4 in.

Figure 5. Graphs of pressure versus loading density for high values of PFP-555



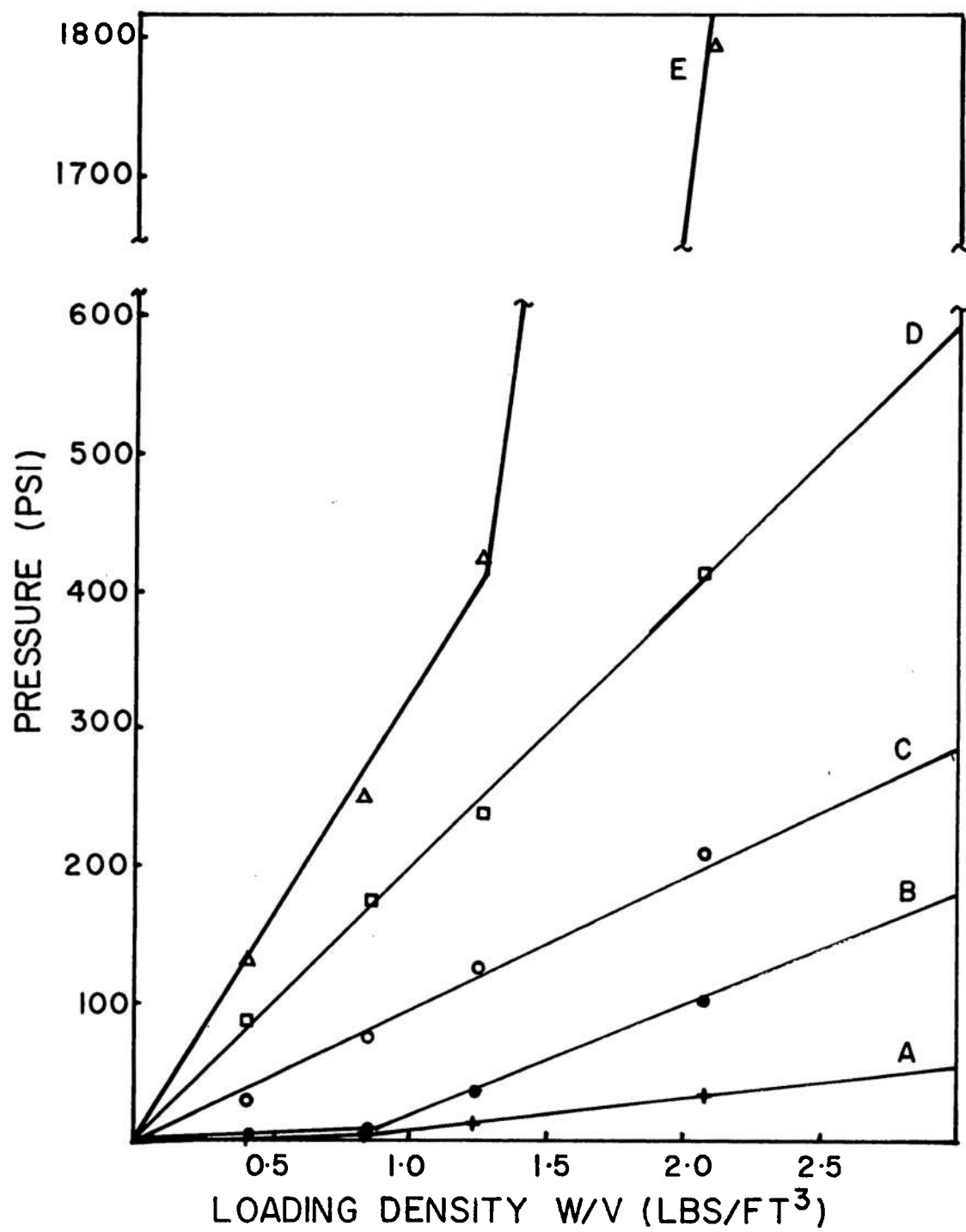
Note: Curves represent the following venting: a = 3 in., b = 2 in., c = 1 in., d = 3/4 in., e = 1/2 in., f = 1/4 in., g = closed.

Figure 6. Graphs of pressure versus loading density for SI-193



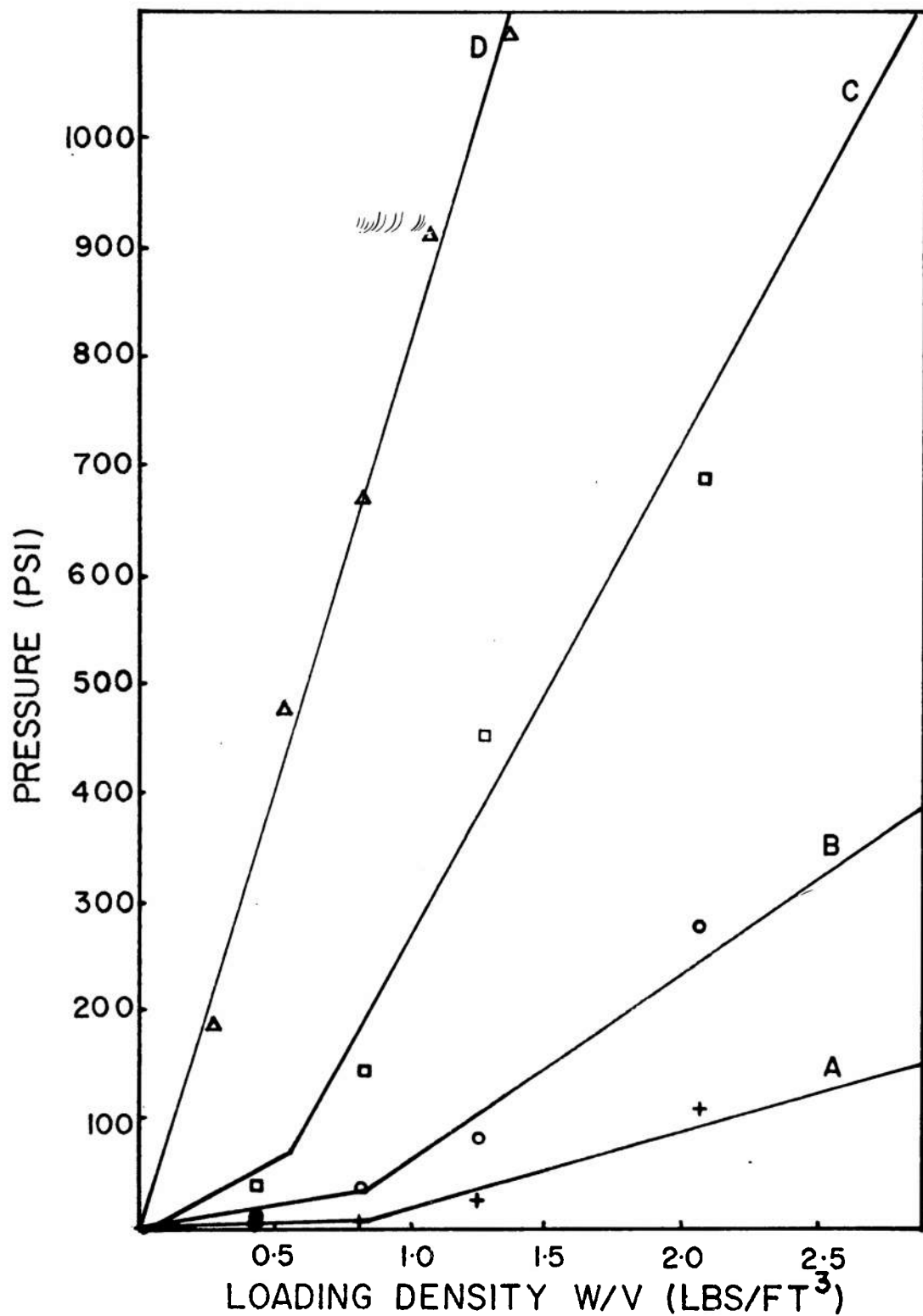
Note: Curves represent the following venting: a = 3 in., b = 2 in., c = 1 in., d = 1/2 in., e = 1/4 in., f = closed.

Figure 7. Graphs of pressure versus loading density for FW-306



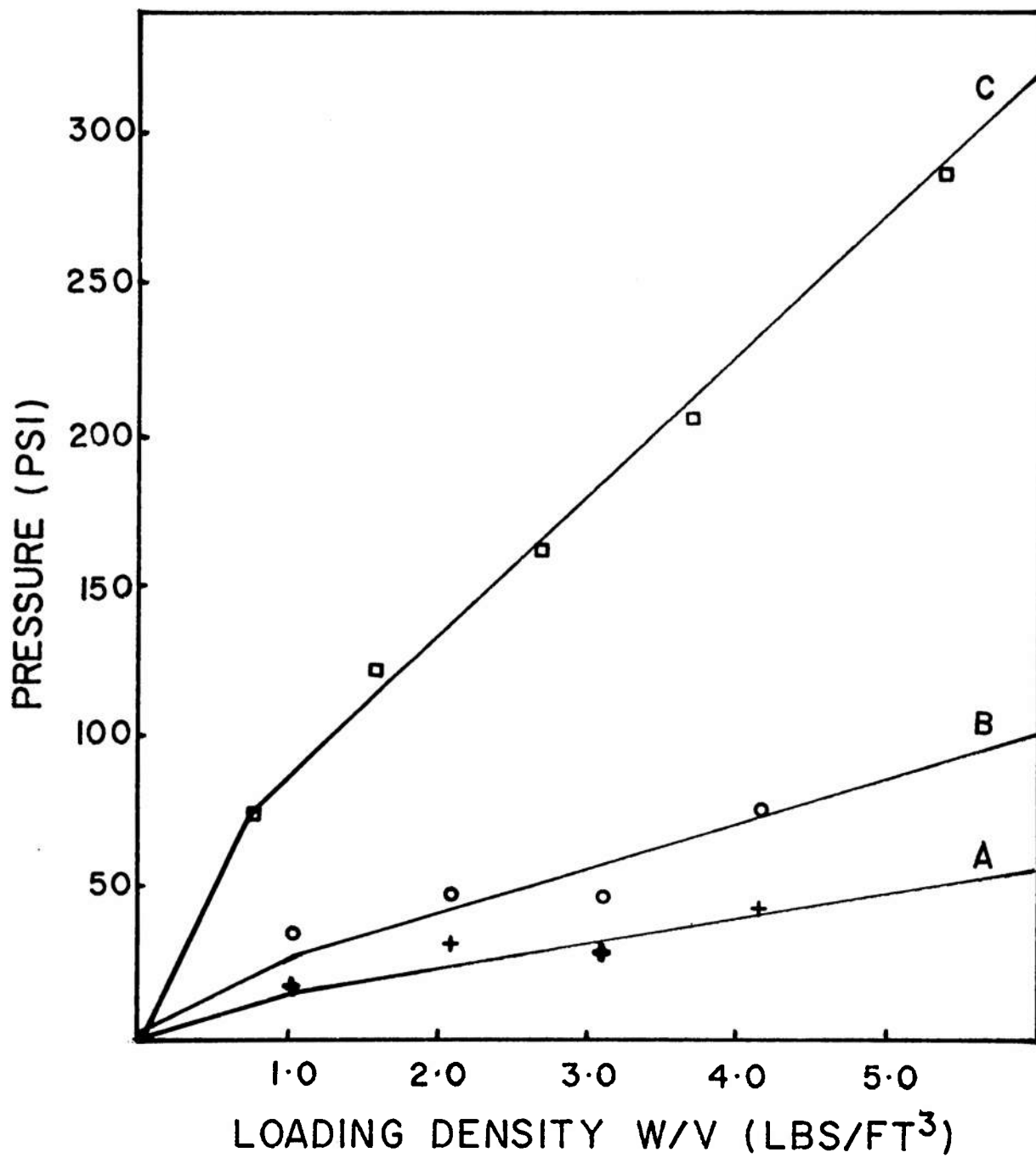
Note: Curves represent the following venting: a = 3 in., b = 2 in.,
 c = 1 in., d = 1/2 in., e = 1/4 in.

Figure 8. Graphs of pressure versus loading density for PFP-555



Note: Curves represent the following venting: a = 3/4 in., b = 1/2 in., c = 1/4 in., d = closed.

Figure 9. Graphs of pressure versus loading density for FY-1451



Note: Curves represent the following venting: a = 1/2 in., b = 1/4 in., c = closed.

Figure 10. Graphs of pressure versus loading density for DP-973

where a and b are constants. Ideally, b should equal zero since p must equal zero when W equals zero. This constraint sometimes forces the p versus W/V curves to assume two distinct slopes. In one case, that of PFP-555 with a 0.6 cm (1/4 in.) vent, the curve (fig. 5) rises more steeply between 30 and 50 g than between 0 and 30 g. However, in the case of 50 g, reaction was much more violent than for smaller weights and the vent plate was blown completely off the vessel.

Table A-1 lists the equations for the straight-line portions of the peak pressure versus loading density (W/V) curves obtained for the various compositions as a function of vent size.

Examining figures 6 through 10, it is seen that the greatest peak pressures were produced by SI-193 followed by FW-306, then PFP-555. Composition FY-1451 gave no pressure inside the vessel for vents 5.0 cm (2 in.) or larger, or for less than 50 g, with a 2.5 cm (1 in.) vent. The peak pressure from this composition for 1.9 cm (3/4 in.) vent was much lower than for SI-193; for 1.3 and 0.6 cm (1/2 and 1/4 in.) vents, it was very low for smaller weights of composition, but approached the values for the other compositions for 50 g samples. The reason for this behavior was the slower burning rate exhibited by these samples, which permitted a larger fraction of gas to escape through the vent, resulting in lower peak pressures. For larger samples, the burning rate becomes great enough to prevent the loss of an appreciable amount of the gas during burning, yielding a higher peak pressure. For the relatively gasless composition DP-973, the peak pressure values were very low for all vents because little gas was produced at all. In fact, no pressure could be obtained for less than 75 g of composition with a 1.9 cm vent, while the pressure was very low (0.25 PSI) with that vent even for 75 and 100 g samples.

Figures 11 through 15 plot the peak pressure versus the log of $A/V^{2/3}$. There is a straight line portion for these curves of the form

$$p = a \ln(A/V^{2/3}) - b \quad (2)$$

with the actual values of a and b given in table A-2. The points depart from a straight line for large vent - small pressure values. The value of a is greatest for FY-1451, because there was a greater percentage of leakage occurring at smaller weights for this composition and the lines rise more steeply than for the others. For DP-973, the weight of the sample seemed to have a rather small effect but the size of the vent a very large effect on the pressure. This was due to the composition reaching a relatively steady state of burning in which gas leaked out as fast as it was produced after an

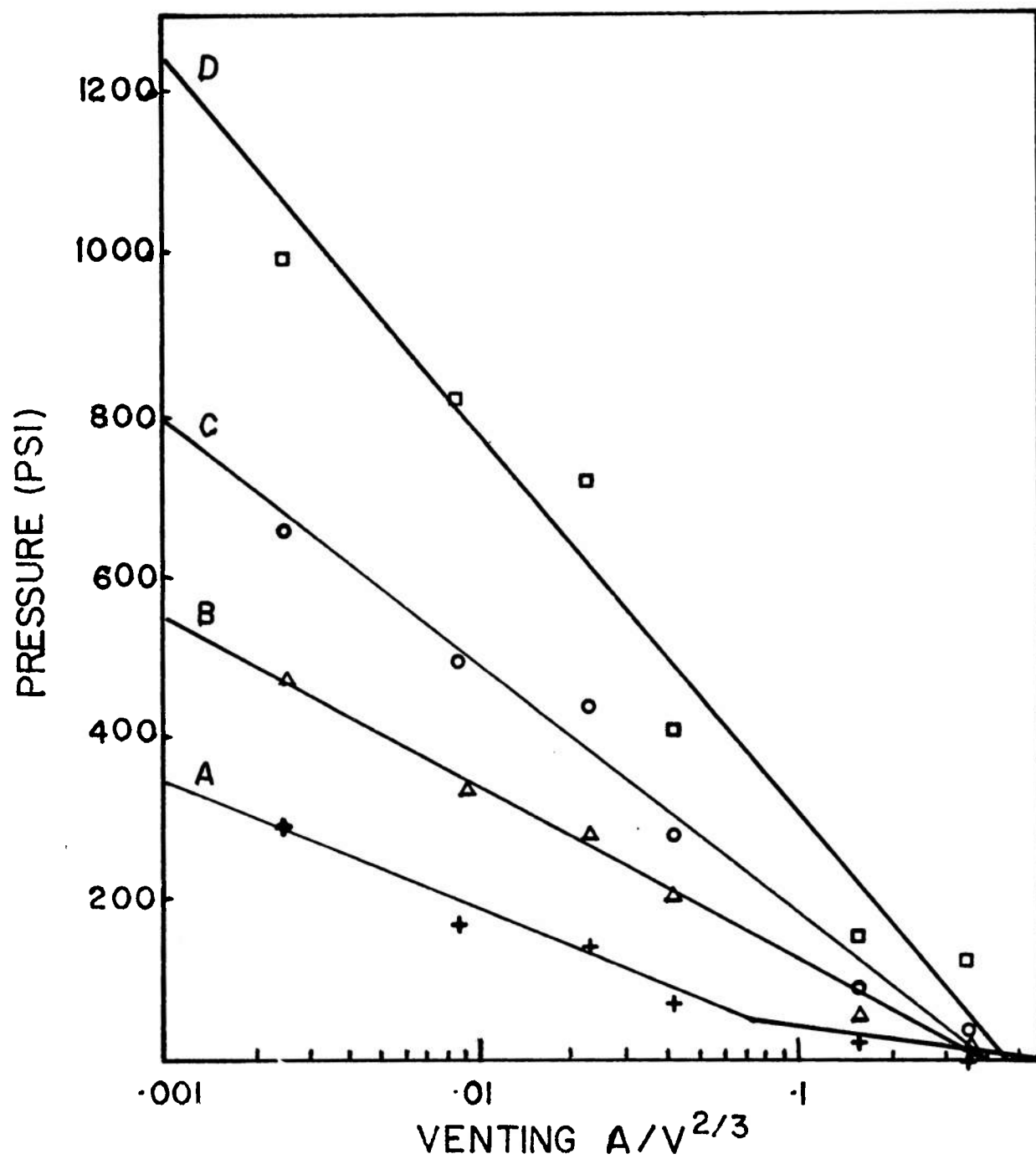


Figure 11. Graphs of pressure versus venting for SI-193

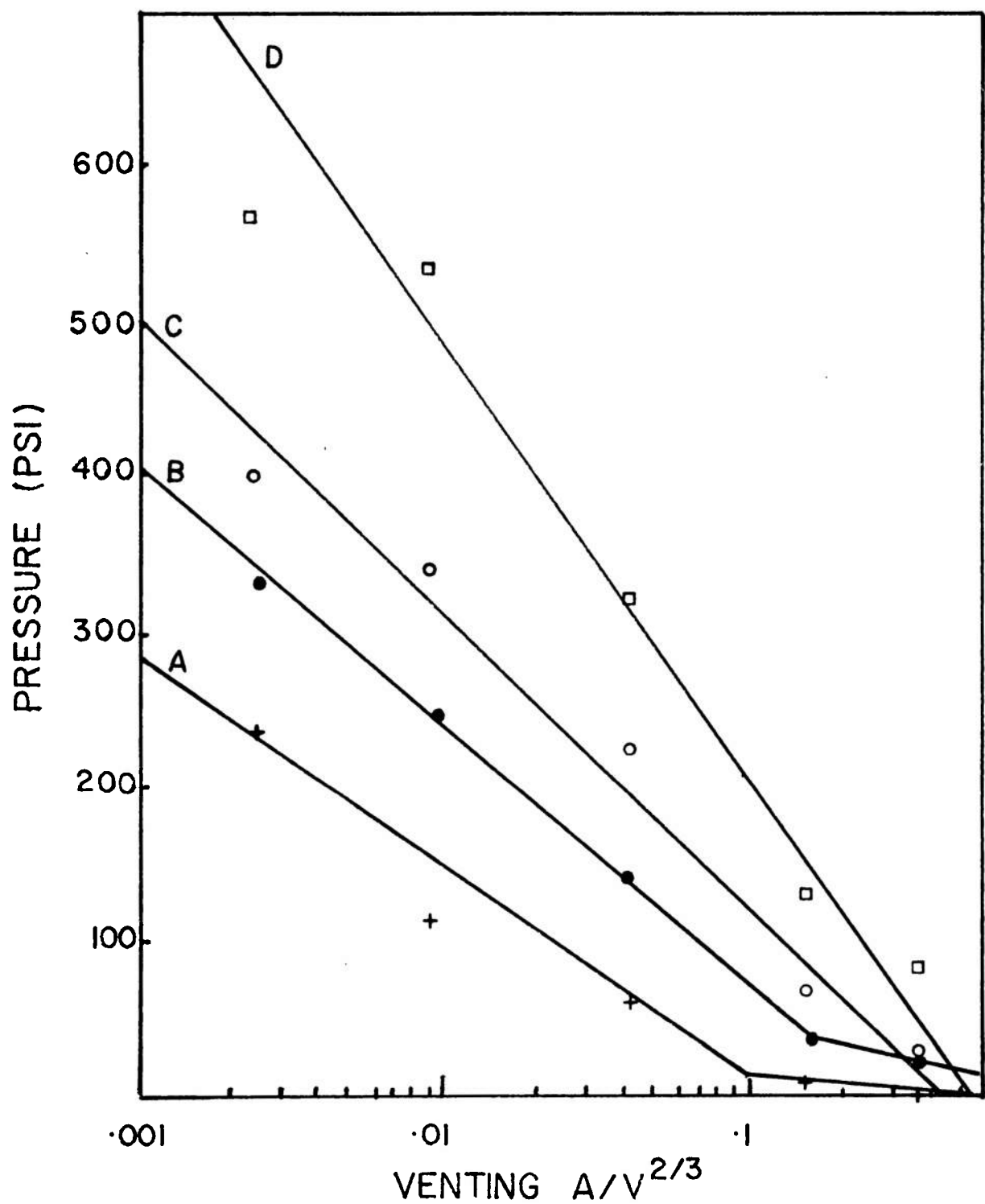
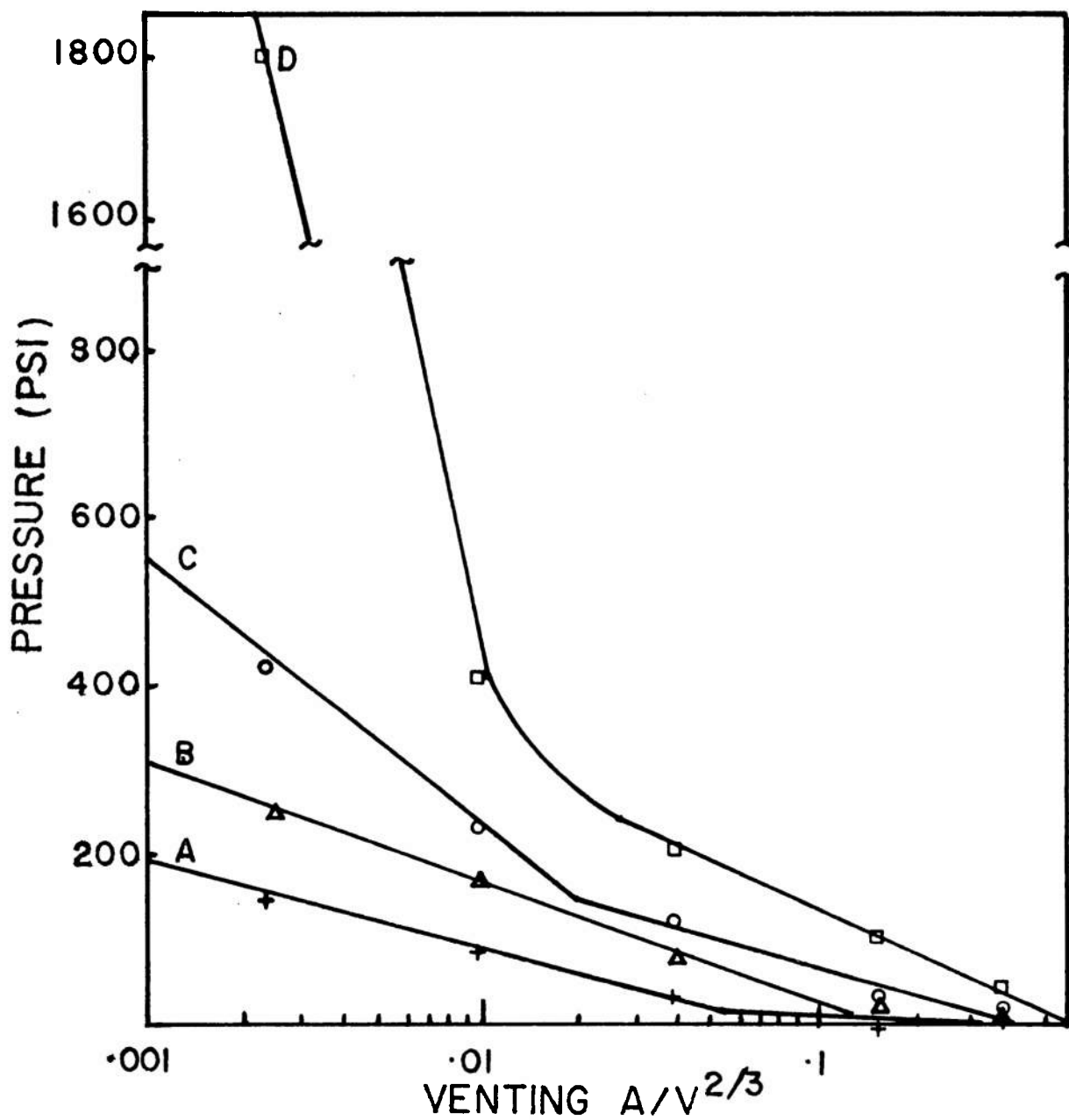
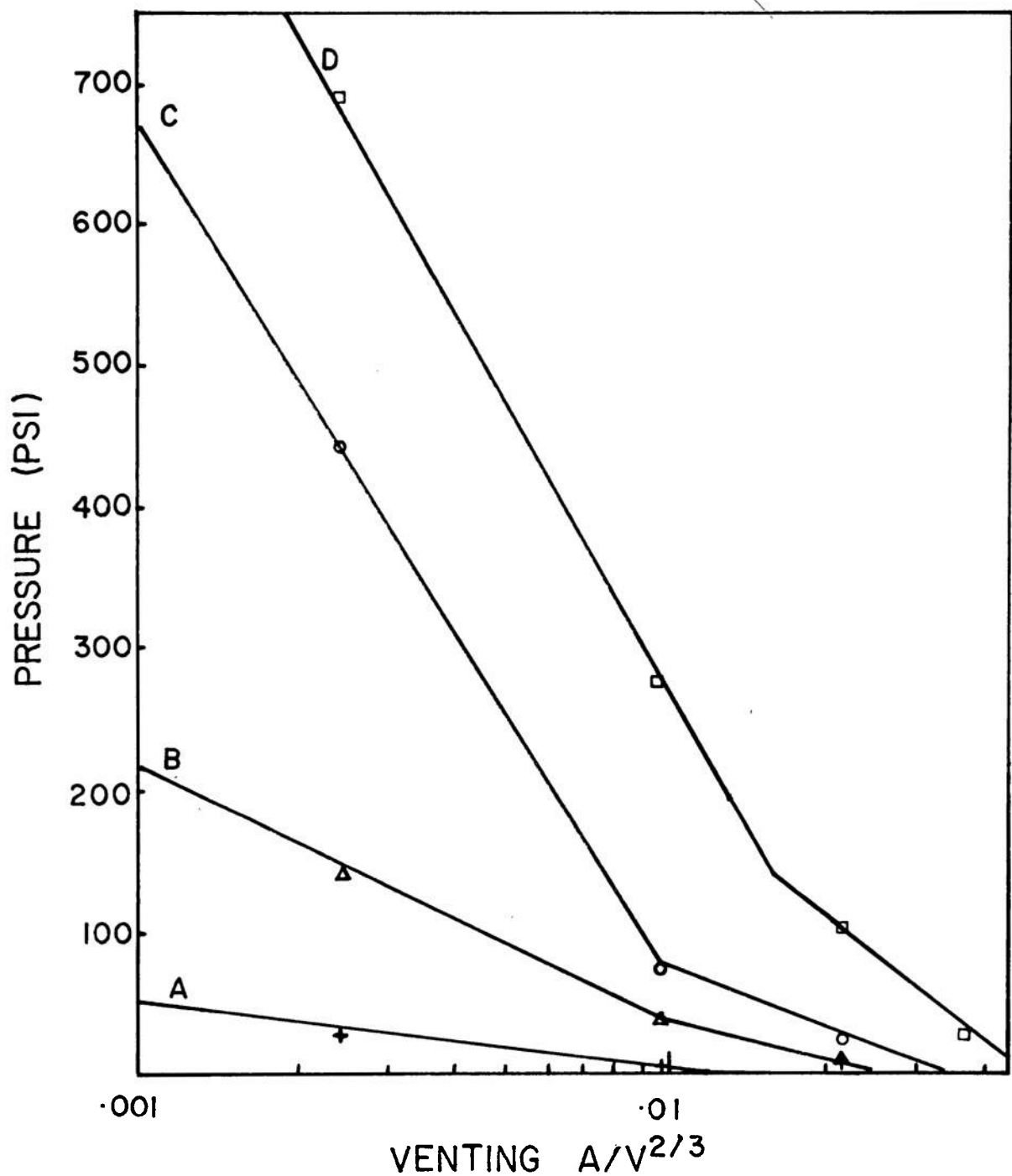


Figure 12. Graphs of pressure versus venting for FW-306



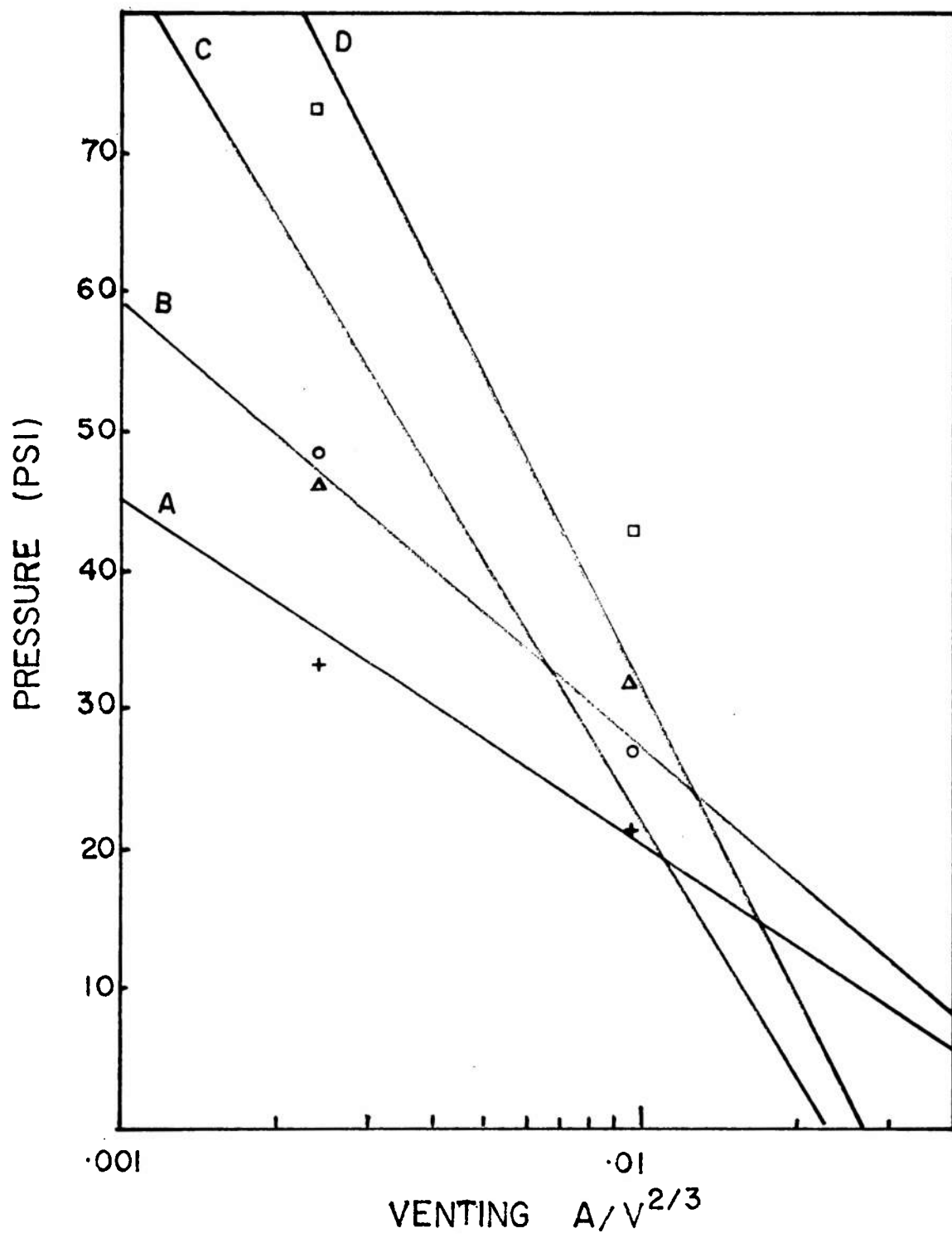
Note: Curves represent the following loading densities: a = 0.416, b = 0.830, c = 1.25, d = 2.08.

Figure 13. Graphs of pressure versus venting for PFP-555



Note: Curves represent the following loading densities: a = 0.416, b = 0.830, c = 1.25, d = 2.08.

Figure 14. Graphs of pressure versus venting for FY-1451



Note: Curves represent the following loading densities: $a = 1.04$, $b = 2.08$, $c = 3.12$, $d = 4.16$.

Figure 15. Graphs of pressure versus venting for DP-973

initial rise. The value reached was simply lower with larger vent areas.

Rate of Pressure Rise (dP/dt) Inside Vessel

In figures 16 through 20, values of dP/dt are plotted versus loading density. Again, the curves have a straight line portion following the equation

$$dP/dt = a W/V + b \quad (3)$$

(table A-3). The values obtained for SI-193 were again highest, followed by FW-306 and PFP-555. Values for FY-1451 were much lower while those of DP-973 were very low. These data illustrated that not only did SI-193 reach higher peak pressures, but also that it reached them in the same time as, or less than, did the others. On the other hand, FY-1451 and DP-973 increased slowly (demonstrated by low dP/dt values) and lost pressure at too great a rate to reach high values.

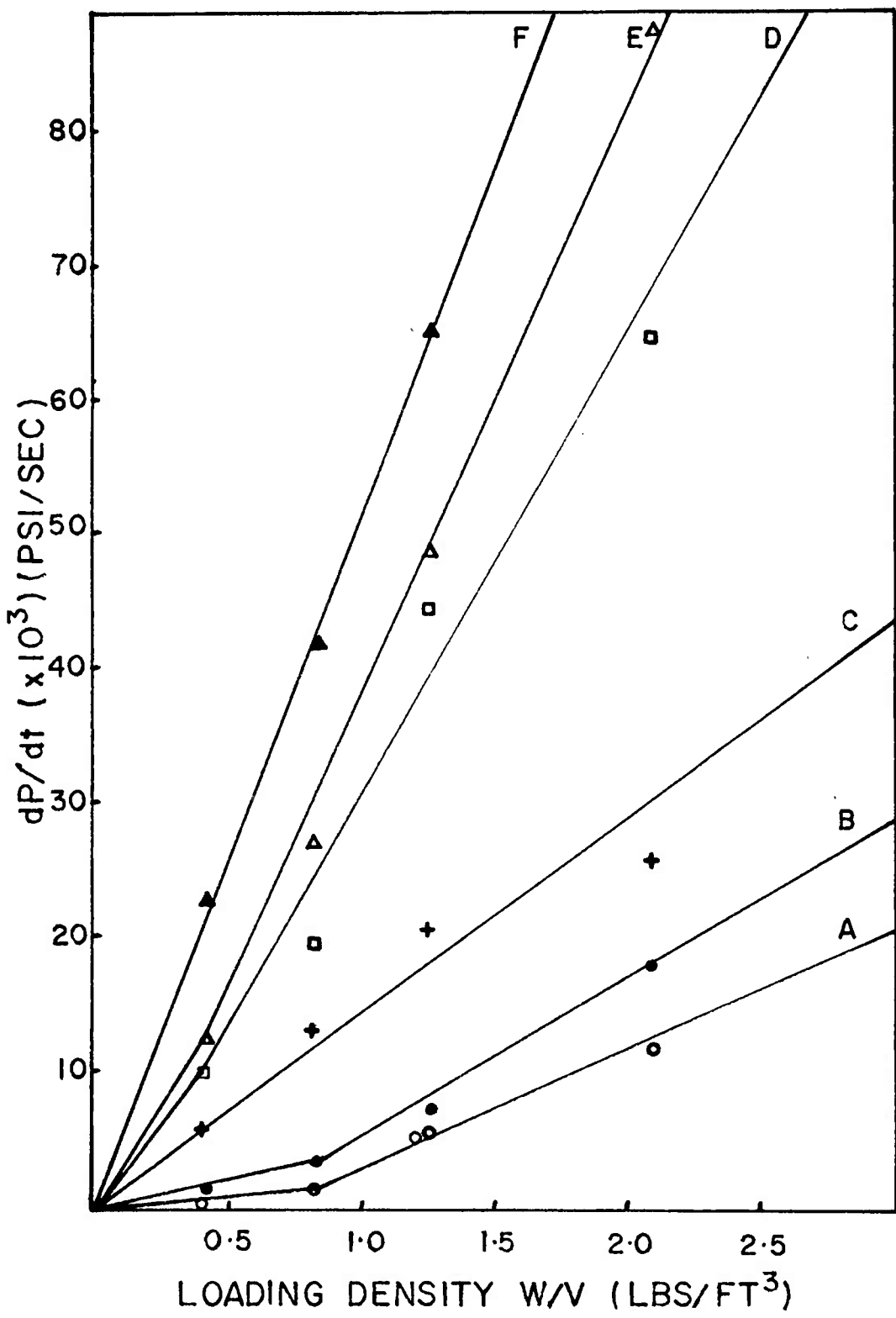
Figures 21 through 25 demonstrate an important phenomenon. In these graphs, the weight of material was held constant while the vent size was varied. If the composition burning rate were not dependent on ambient pressure, the values would not change with vent size and the lines would be horizontal. This was not the case; there are a series of lines of the form

$$dP/dt = - a \ln(A/V^{2/3}) - b \quad (4)$$

(table A-4), in which dP/dt increases as vent size becomes smaller. This increase in dP/dt most assuredly resulted from increased transfer of thermal energy to the reacting composition. This transfer occurred because of the reduction of the mean free path with increasing pressure and consequent reduction in the diffusion of hot atoms and molecules from the vicinity of the reacting surface. Furthermore, dP/dt may be increased by containing the flame within the vessel by the smaller vents (confirmed by photographs) thereby increasing the amount of energy transferred by radiation. The fact that the burning rate of consolidated pyrotechnic compositions is pressure dependent is well known (refs 6,7). With increasing altitude (decreasing pressure), the burning rate of flares decreases significantly because of the rapid diffusion from the reaction zone of hot gases consisting of both active species and products.

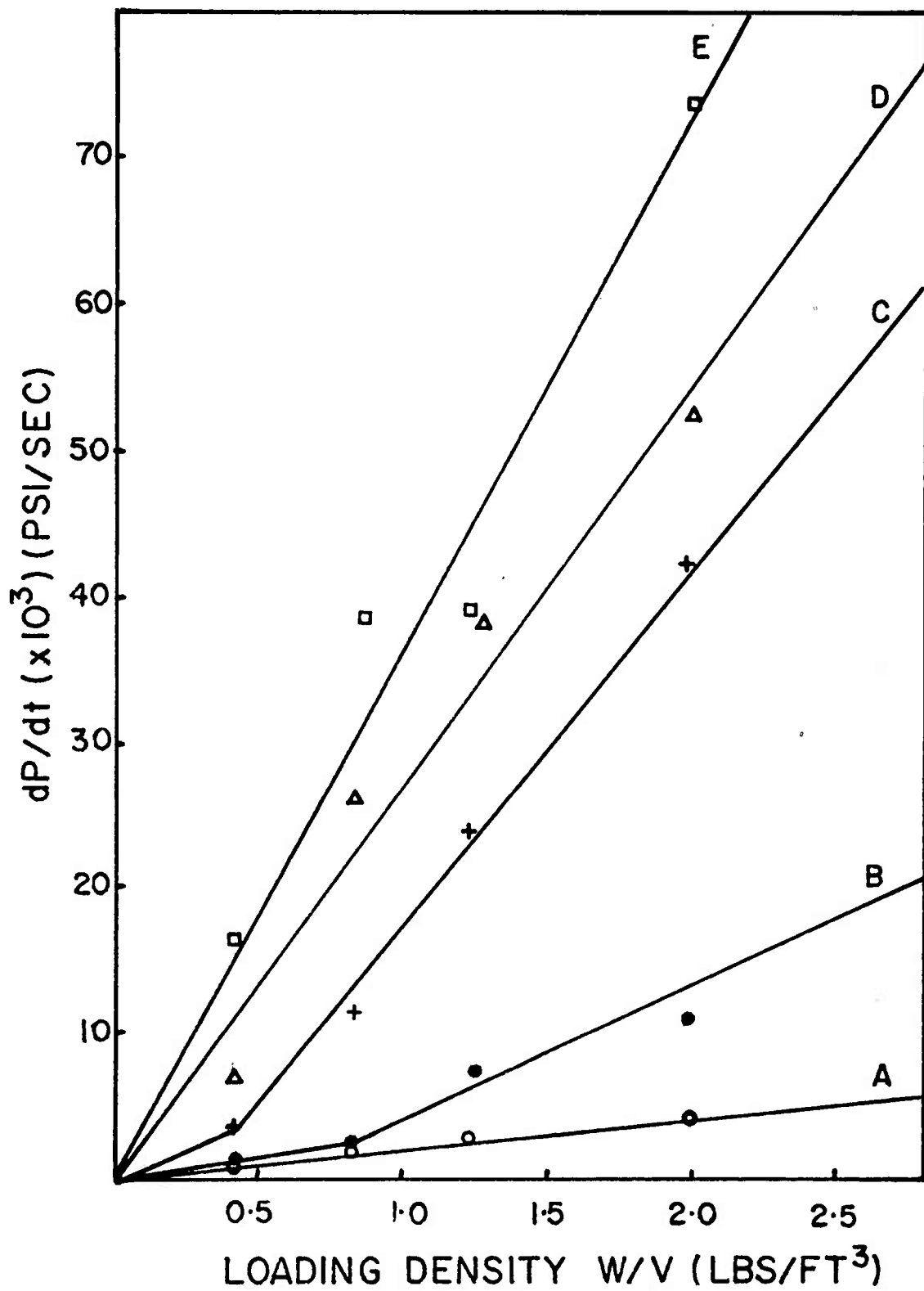
Scaled Impulse Inside Vessel

The scaled impulse ($i/W^{1/3}$) is plotted versus scaled vent areas ($A/W^{2/3}$) in figures 26 through 30. The curves show a common straight



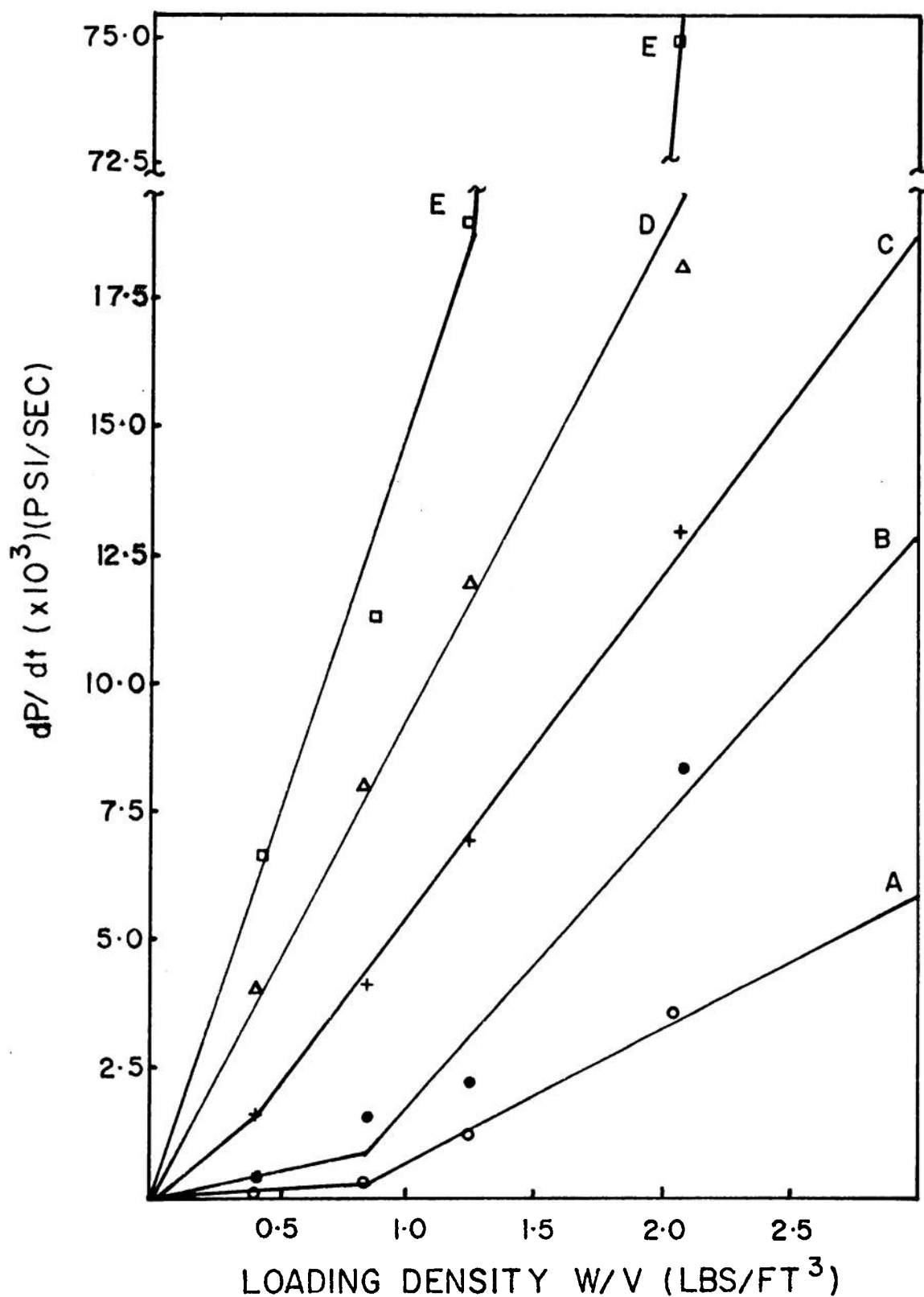
Note: Curves represent the following venting: a = 3 in., b = 2 in., c = 1 in., d = 3/4 in., e = 1/2 in., f = 1/4 in.

Figure 16. Graphs of dP/dt versus loading density for SI-193



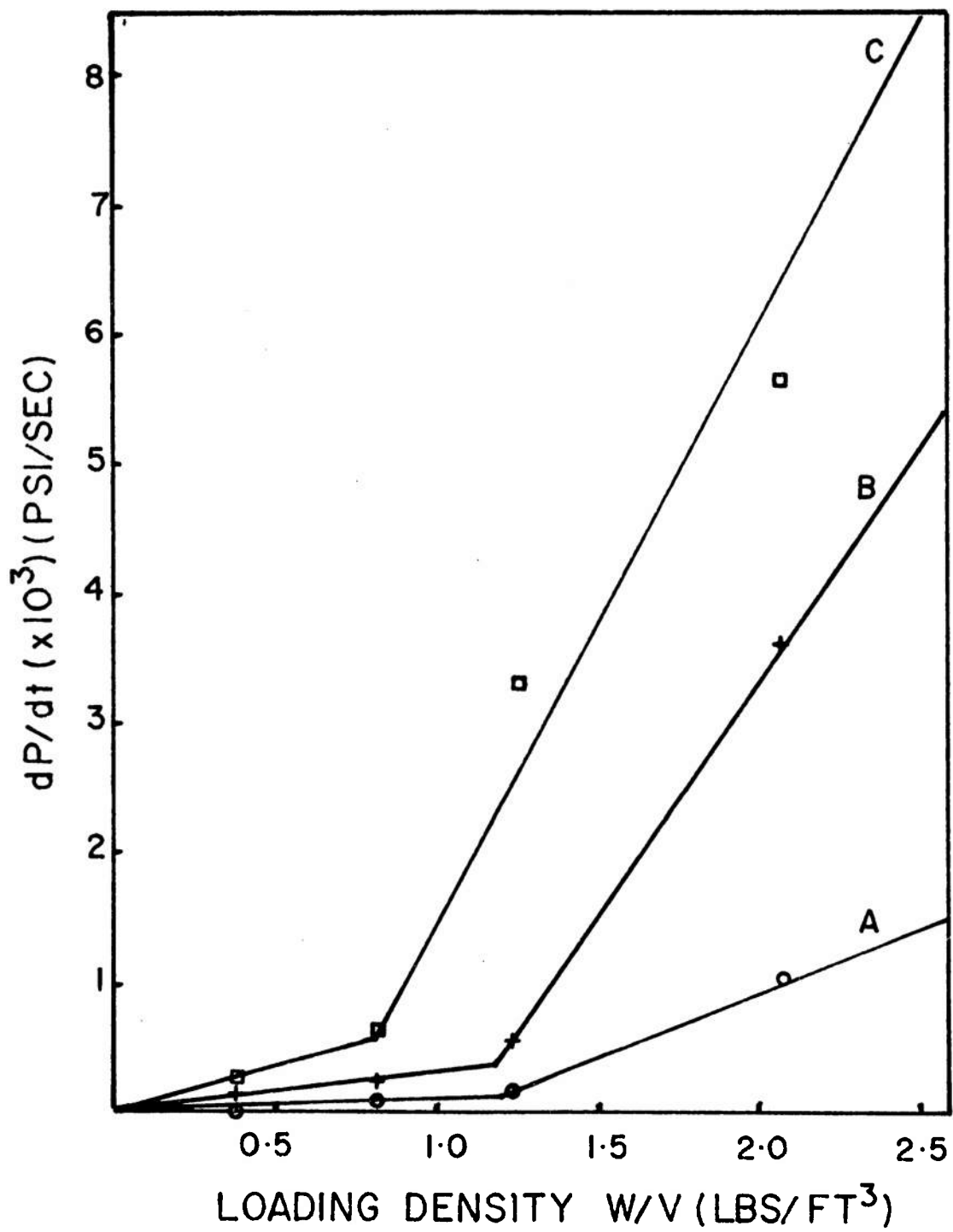
Note: Curves represent the following venting: a = 3 in., b = 2 in., c = 1 in., d = 1/2 in., e = 1/4 in.

Figure 17. Graphs of dP/dt versus loading density for FW-306



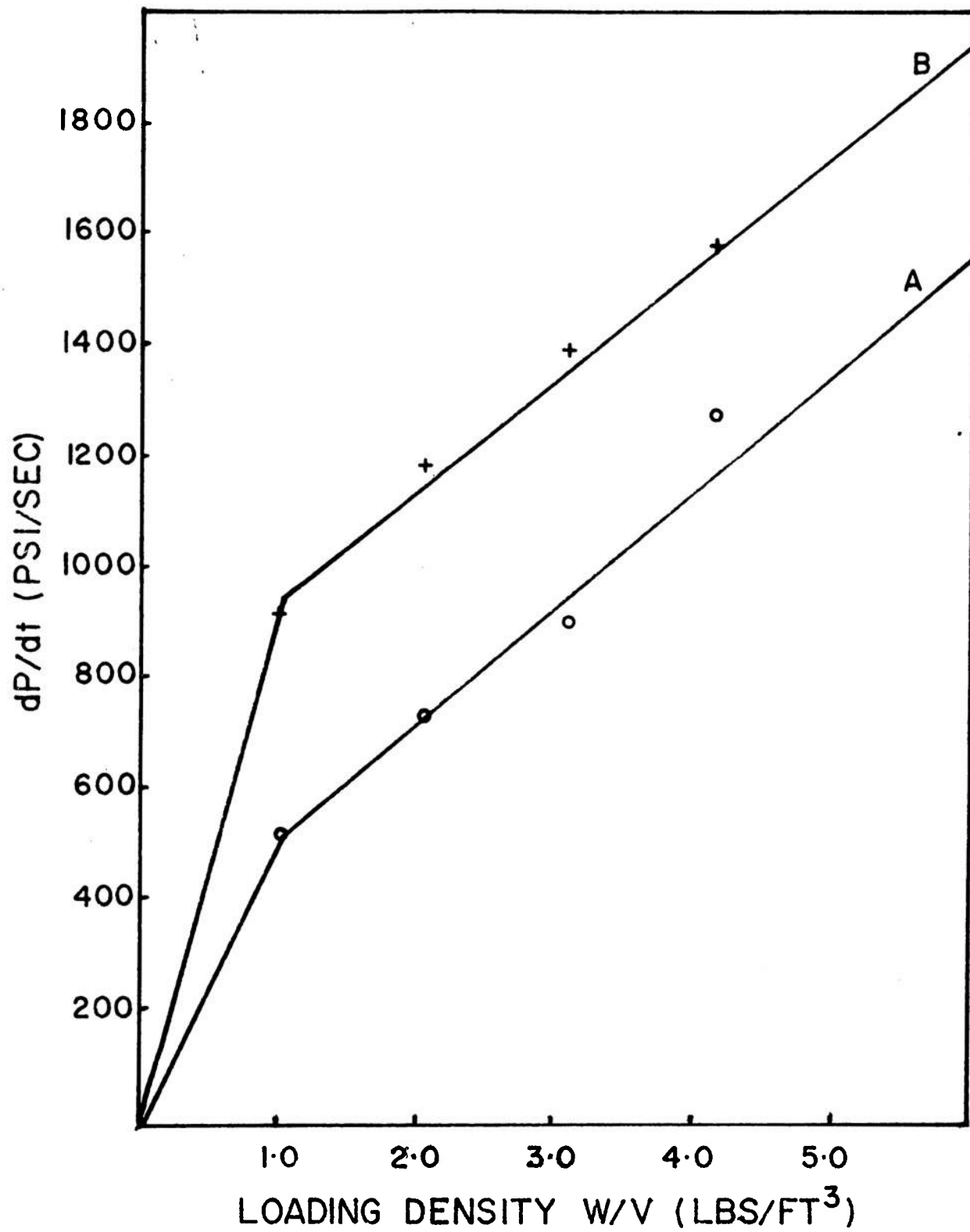
Note: Curves represent the following venting: a = 3 in., b = 2 in., c = 1 in., d = 1/2 in., e = 1/4 in.

Figure 18. Graphs of dP/dt versus loading density for PFP-555



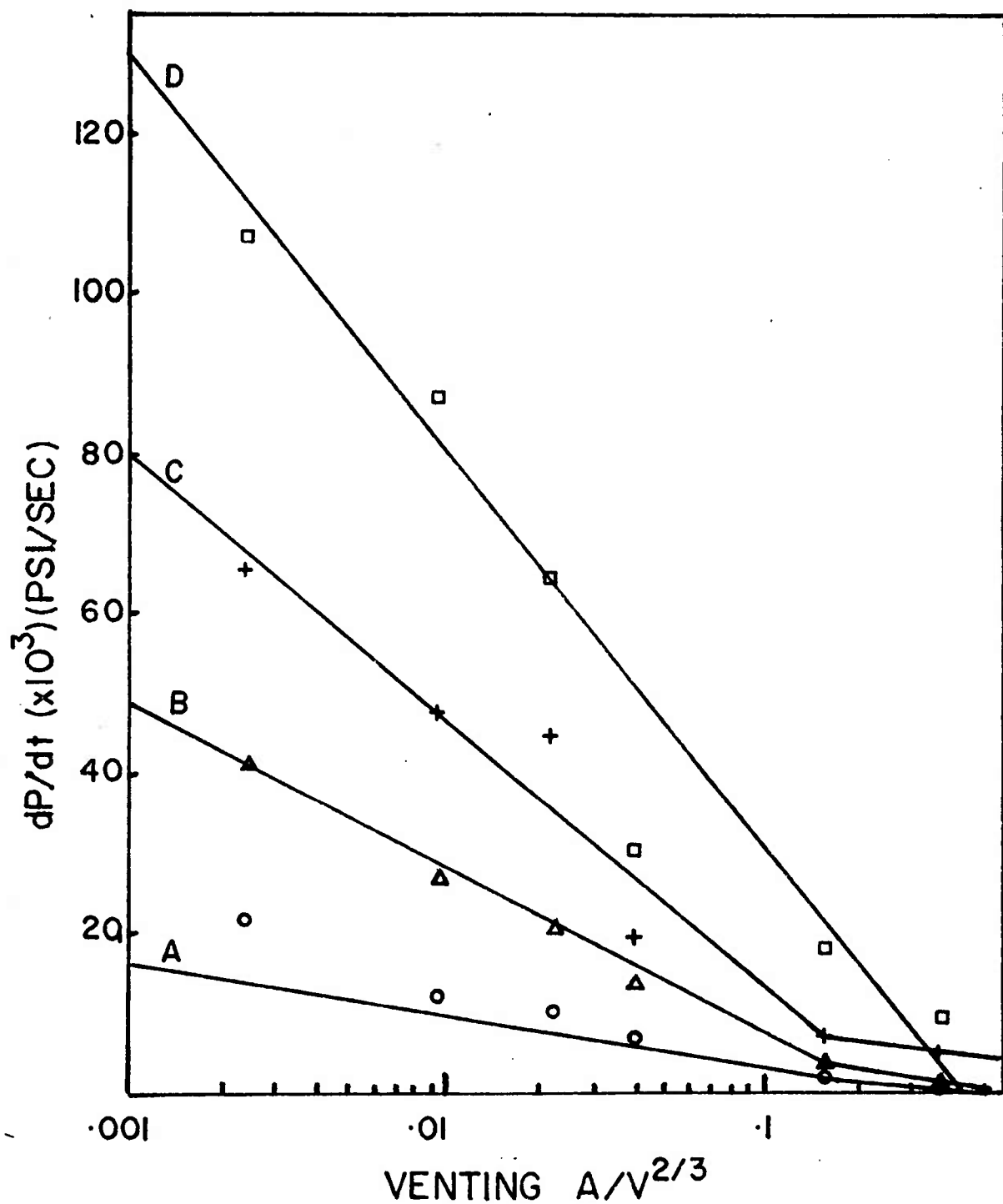
Note: Curves represent the following venting: a = 3/4 in., b = 1/2 in., c = 1/4 in.

Figure 19. Graphs of dP/dt versus loading density for FY-1451



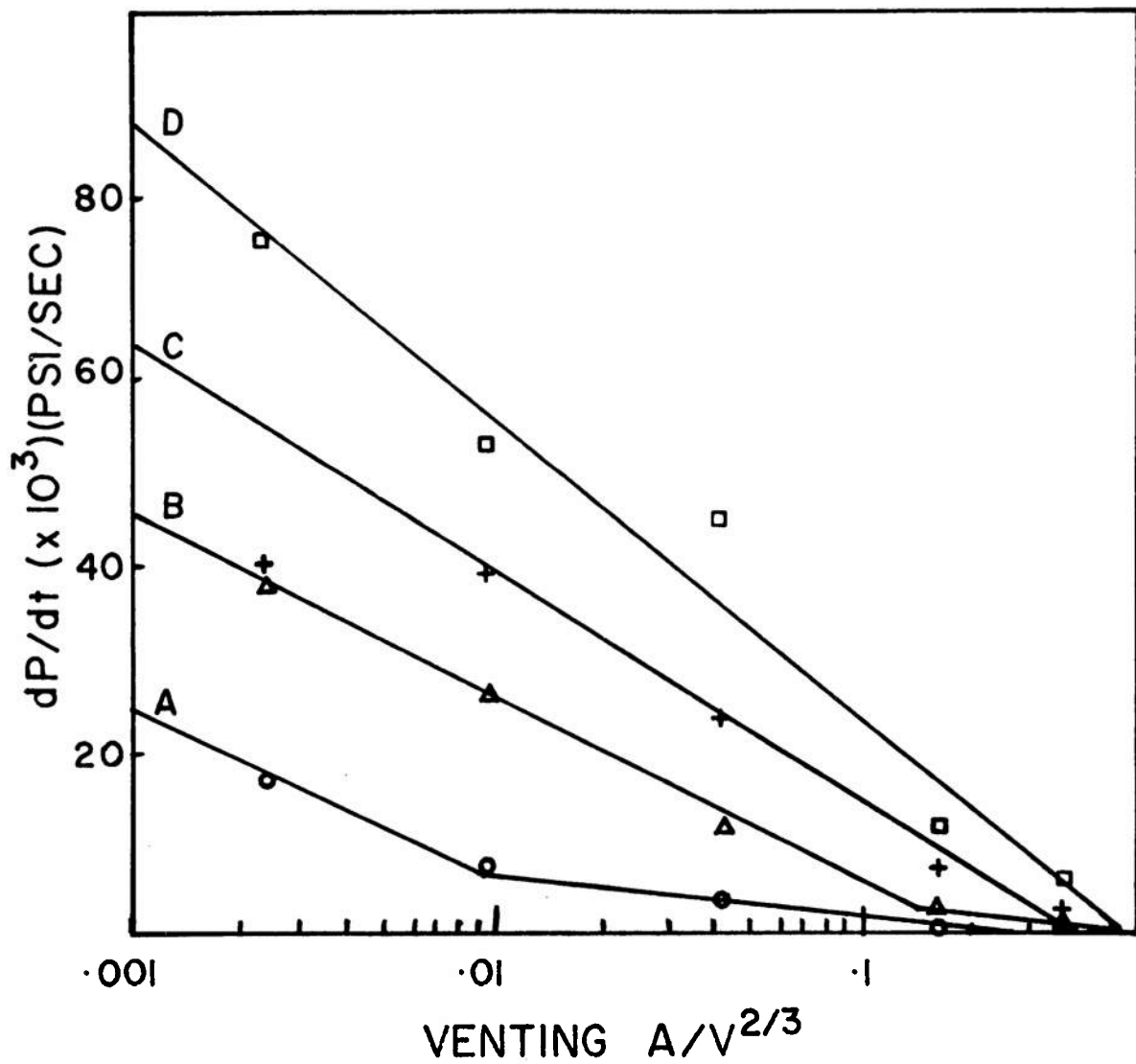
Note: Curves represent the following venting: $a = 1/2$ in., $b = 1/4$ in.

Figure 20. Graphs of dP/dt versus loading density for DP-973



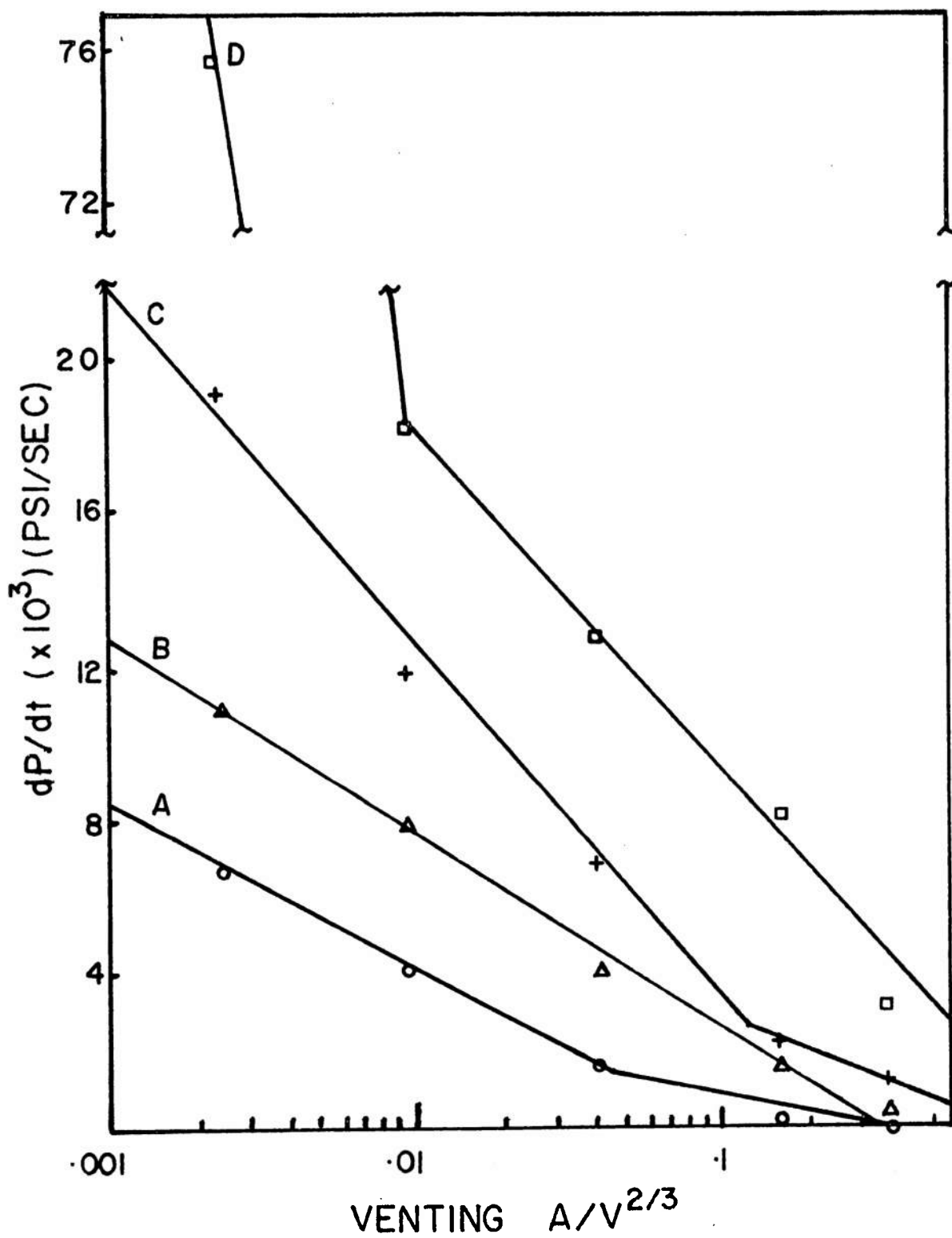
Note: Curves represent the following loading densities: $a = 0.416$, $b = 0.830$, $c = 1.25$, $d = 2.08$.

Figure 21. Graphs of dP/dt versus venting for SI-193



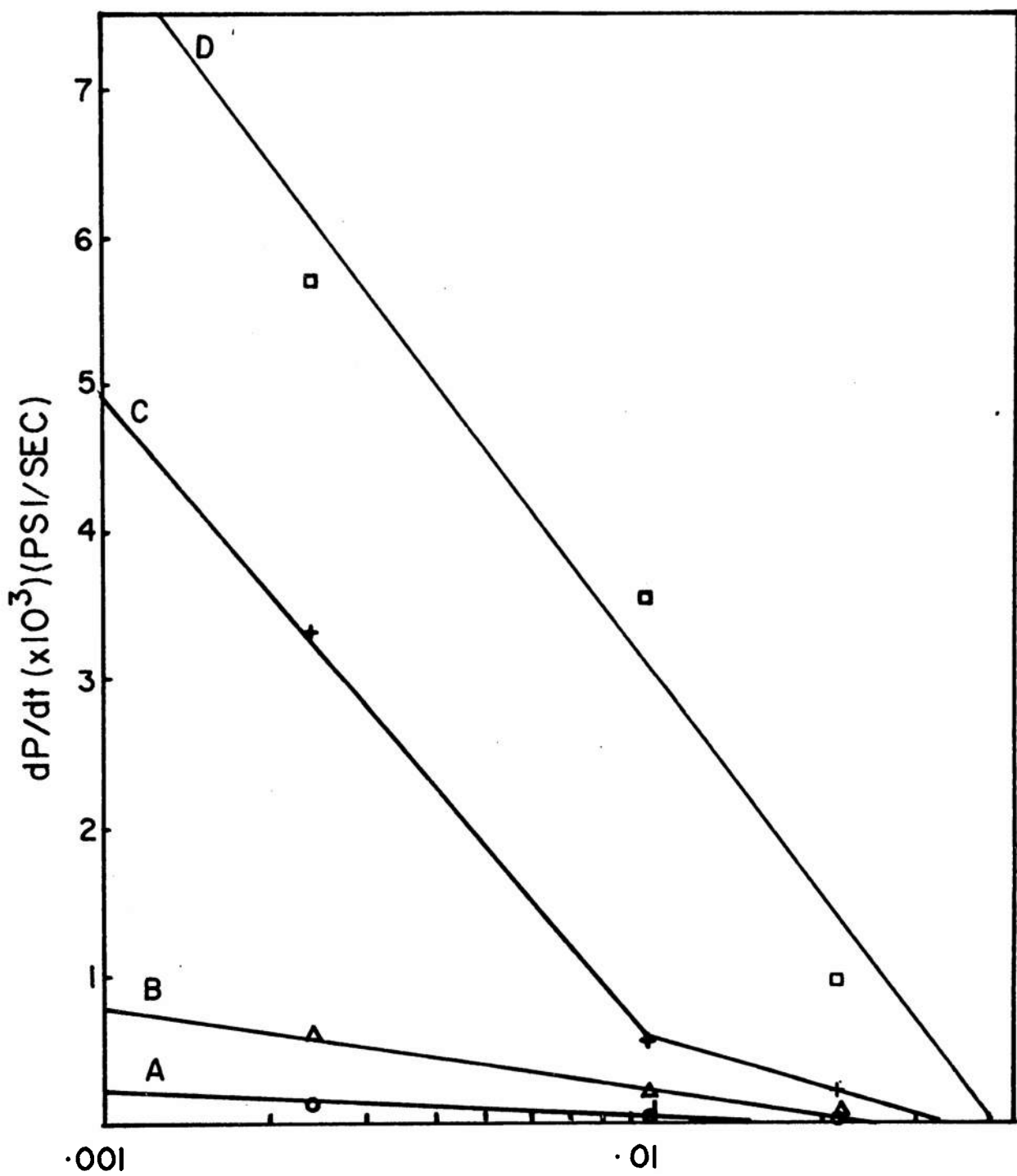
Note: Curves represent the following loading densities:
 $a = 0.416$, $b = 0.830$, $c = 1.25$, $d = 2.08$.

Figure 22. Graphs of dP/dt versus venting for FW-306



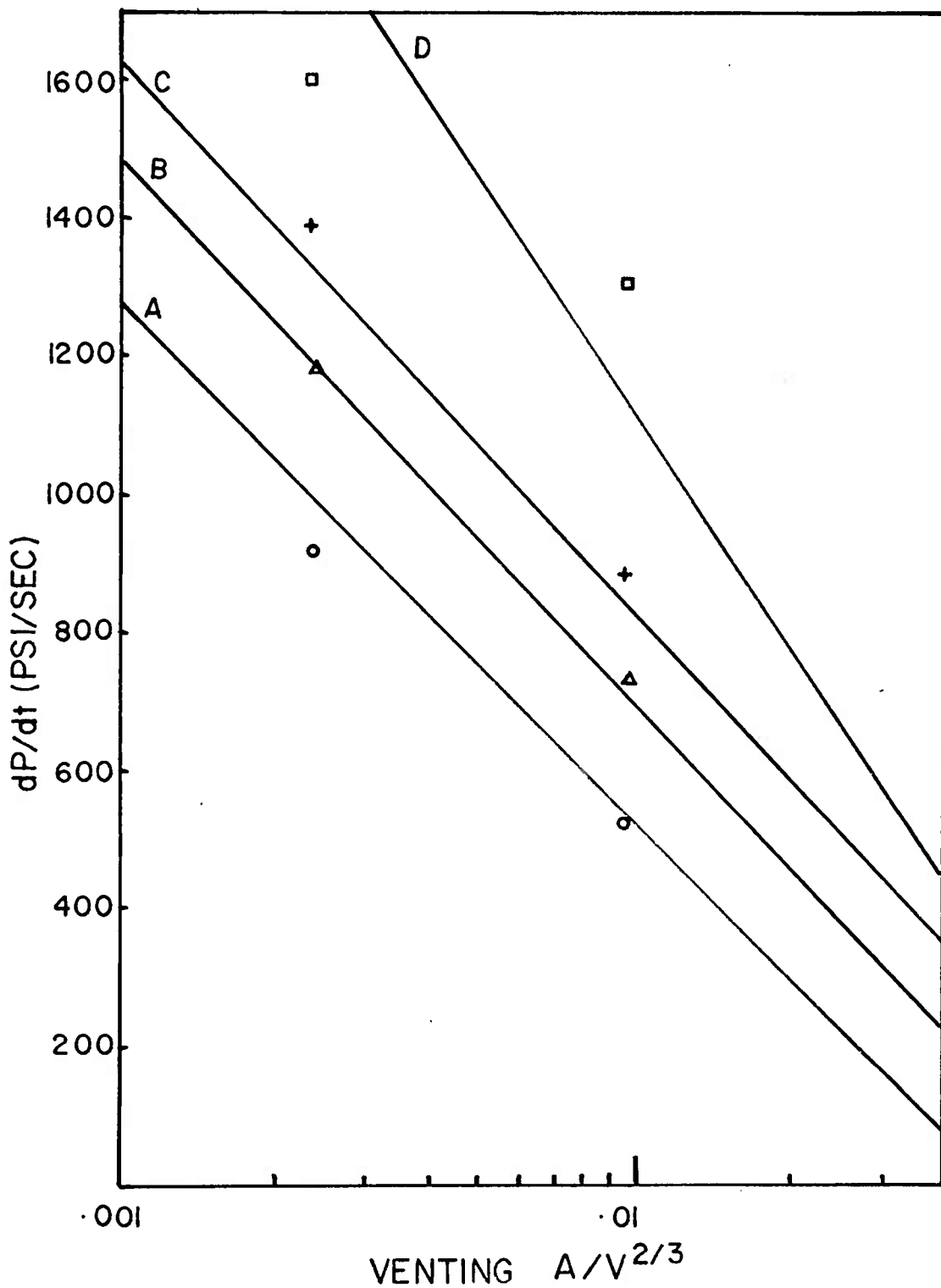
Note: Curves represent the following loading densities:
 $a = 0.416$, $b = 0.830$, $c = 1.25$, $d = 2.08$.

Figure 23. Graphs of dP/dt versus venting for PFP-555



Note: Curves represent the following loading densities:
 $a = 0.416$, $b = 0.830$, $c = 1.25$, $d = 2.08$.

Figure 24. Graphs of dP/dt versus venting for FY-1451



Note: Curves represent the following loading densities: $a = 1.04$, $b = 2.08$, $c = 3.12$, $d = 4.16$.

Figure 25. Graphs of dP/dt versus venting for DP-973

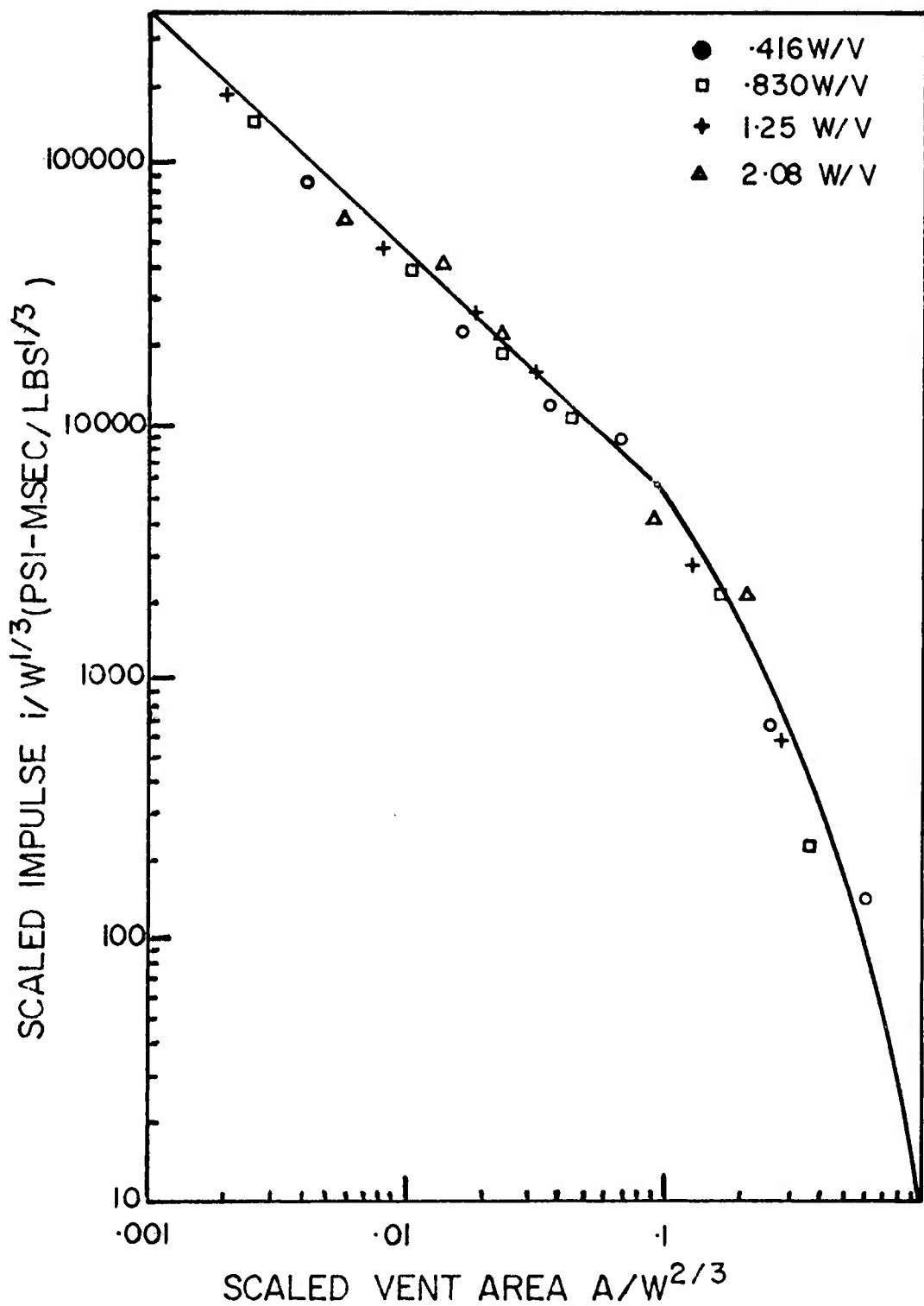


Figure 26. Graphs of scaled impulse versus scaled vent area for SI-193

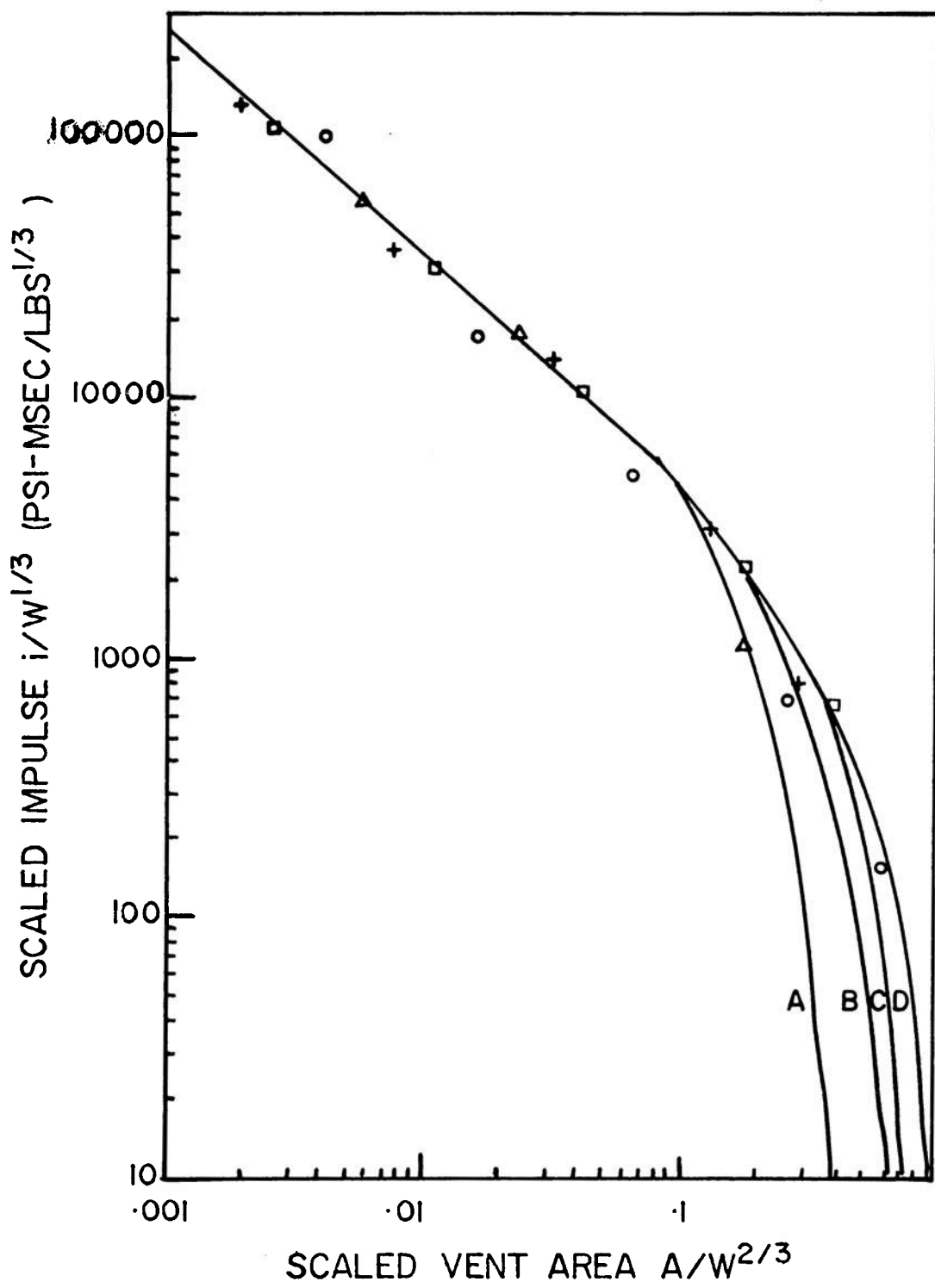


Figure 27. Graphs of scaled impulse versus scaled vent area for FW-306

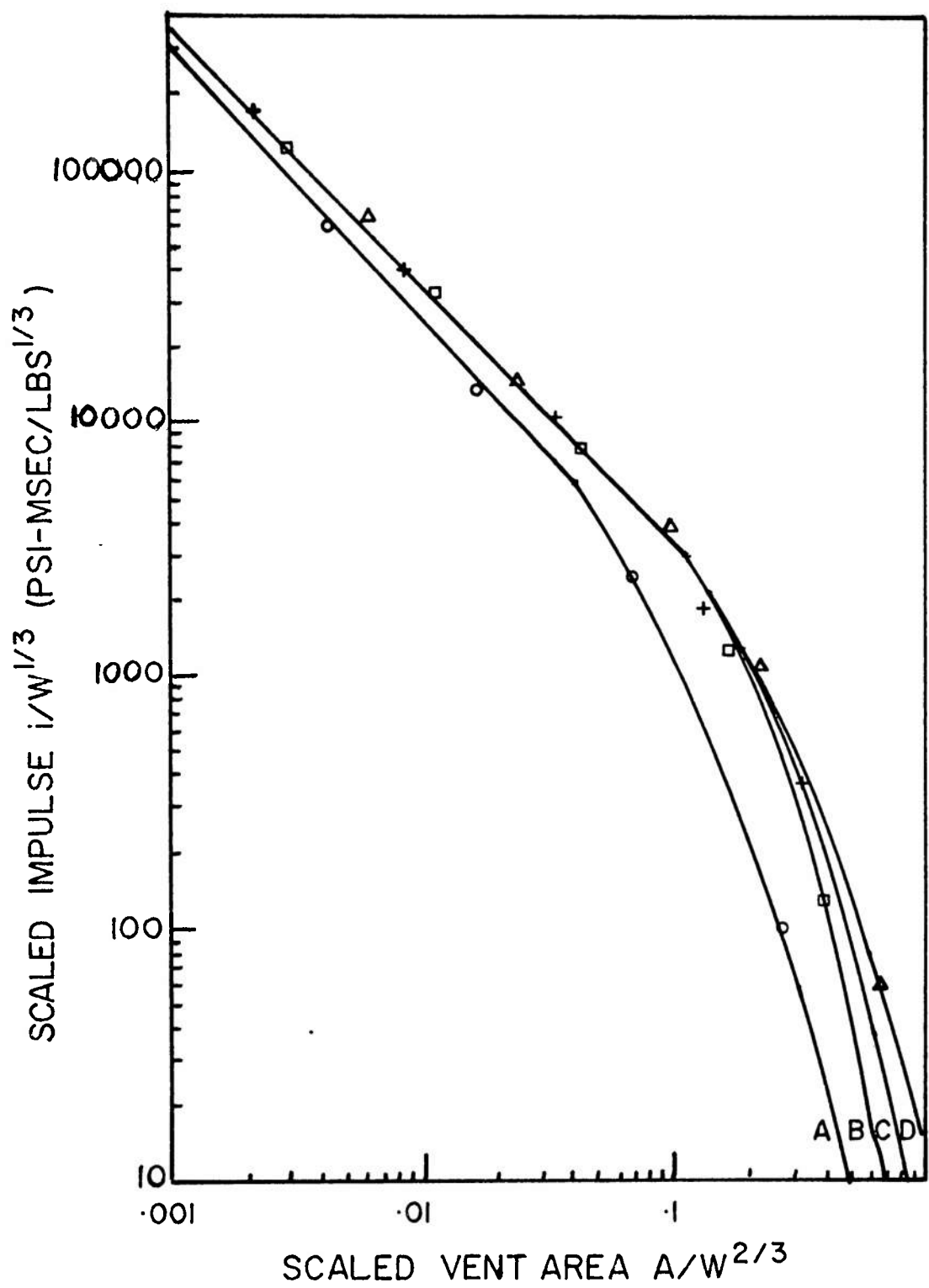


Figure 28. Graphs of scaled impulse versus scaled vent area for PFP-555

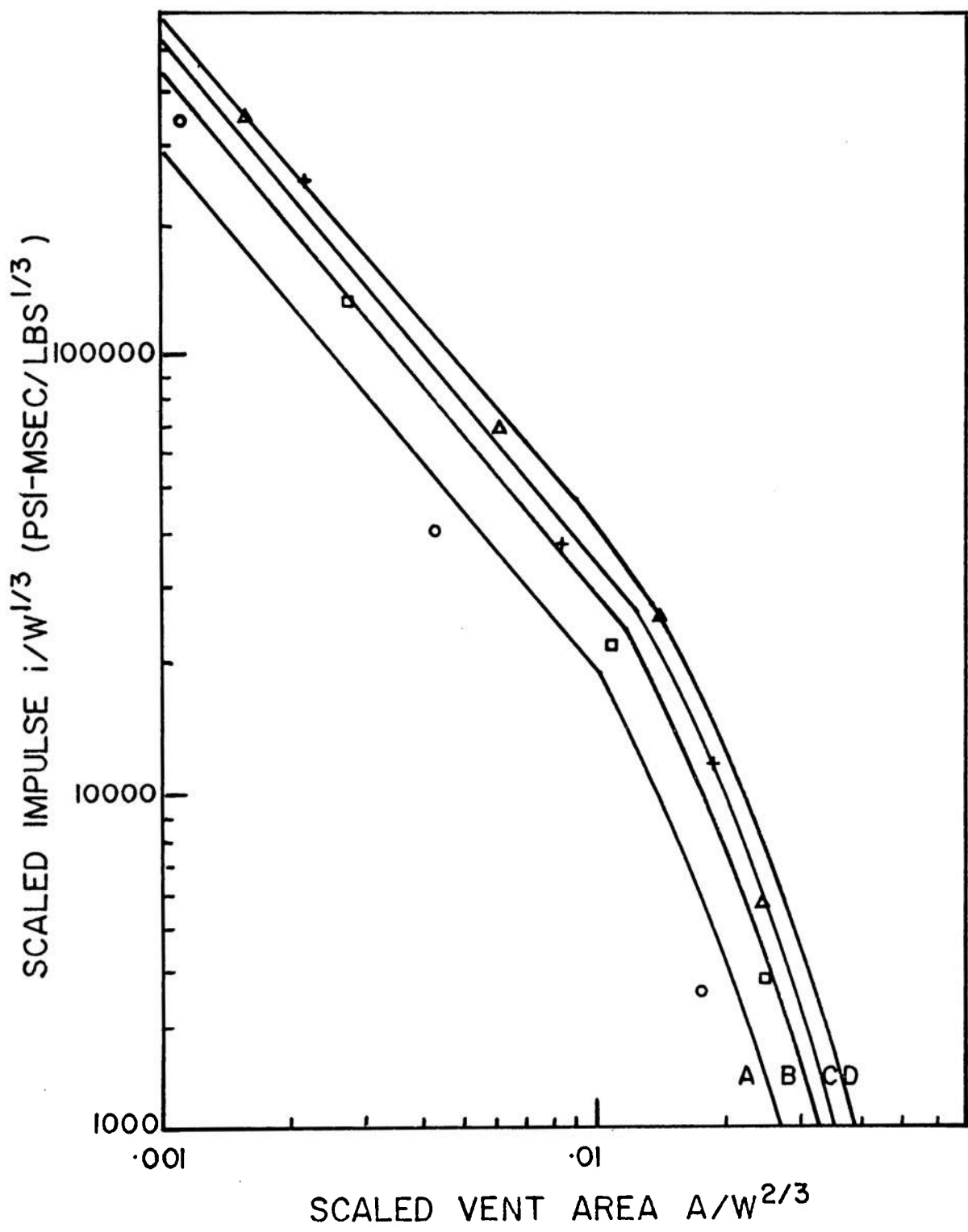


Figure 29. Graphs of scaled impulse versus scaled vent area for FY-1451

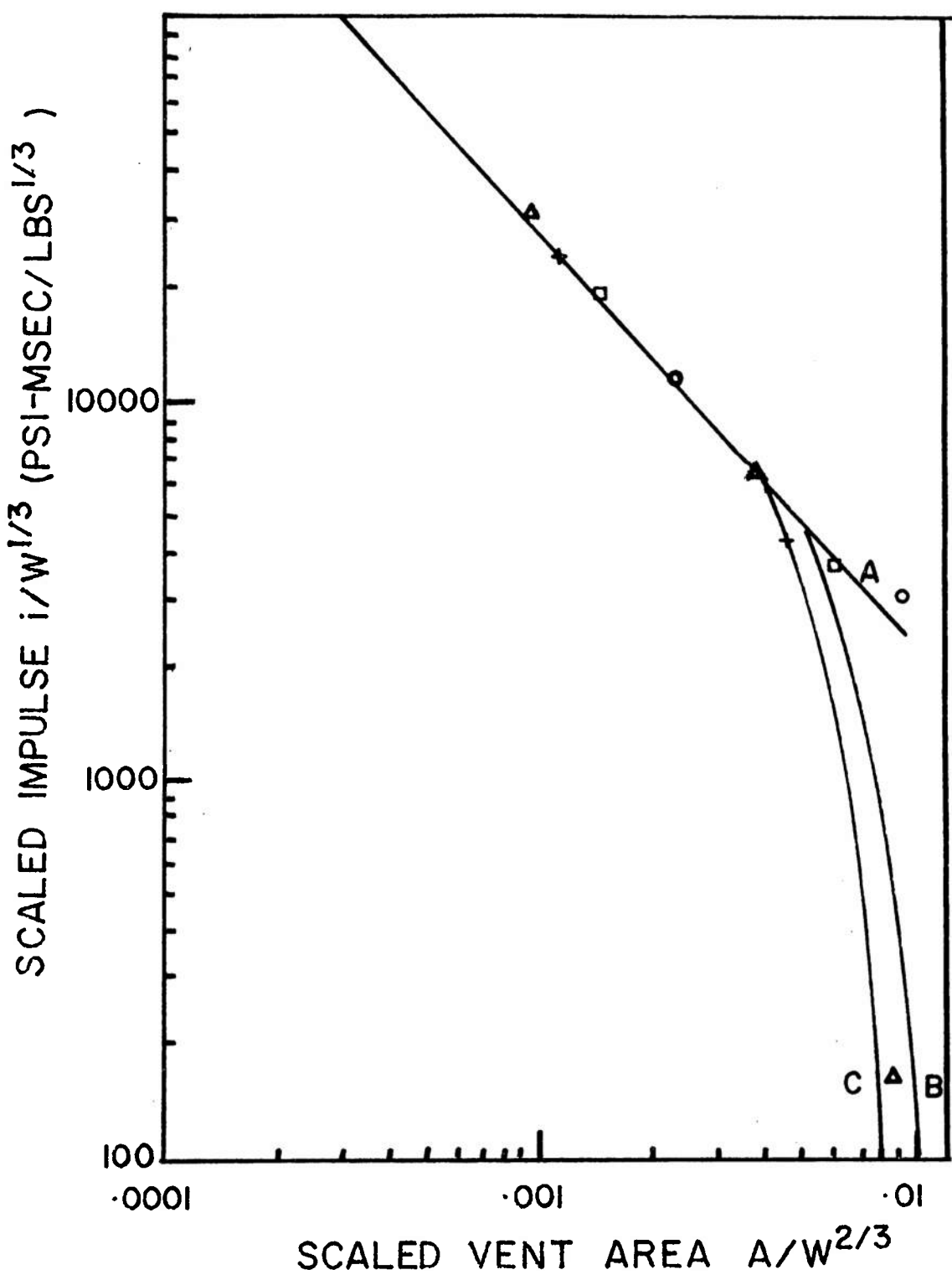


Figure 30. Graphs of scaled impulse versus scaled vent area for DP-973

line portion, which becomes a family of curves for $A/V^{2/3} > 0.0387$, for SI-193, PFP-555, and FW-306. The equation for the straight line portion is

$$i/W^{1/3} = b (A/W^{2/3})^a \quad (5)$$

(table A-5). It appears that at this vent area, the degree of venting changed. These curves are similar in shape to those for explosives (ref 1), except that here there is a common straight line portion rather than a different one for each weight of composition.

For FY-1451, there is a family of curves which departs from straight lines for $A/V^{2/3} > 0.00968$. The equation for these straight lines takes the form

$$i/W^{1/3} = a (A/W^{2/3})^b (W/V)^c \quad (6)$$

Since this composition reached a much lower pressure more slowly, it is reasonable that it would not feel the effect of reducing vent size until a smaller vent is reached. The loading density (W/V) also had more of an effect on impulse for this composition than for the others, since exponent c is zero in equation 5.

The curve for DP-973 falls off at around $A/V^{2/3} = 0.00968$; however, with only one point beyond the straight line section, it is difficult to determine what was occurring.

Scaled Duration of Pressure Inside Vessel

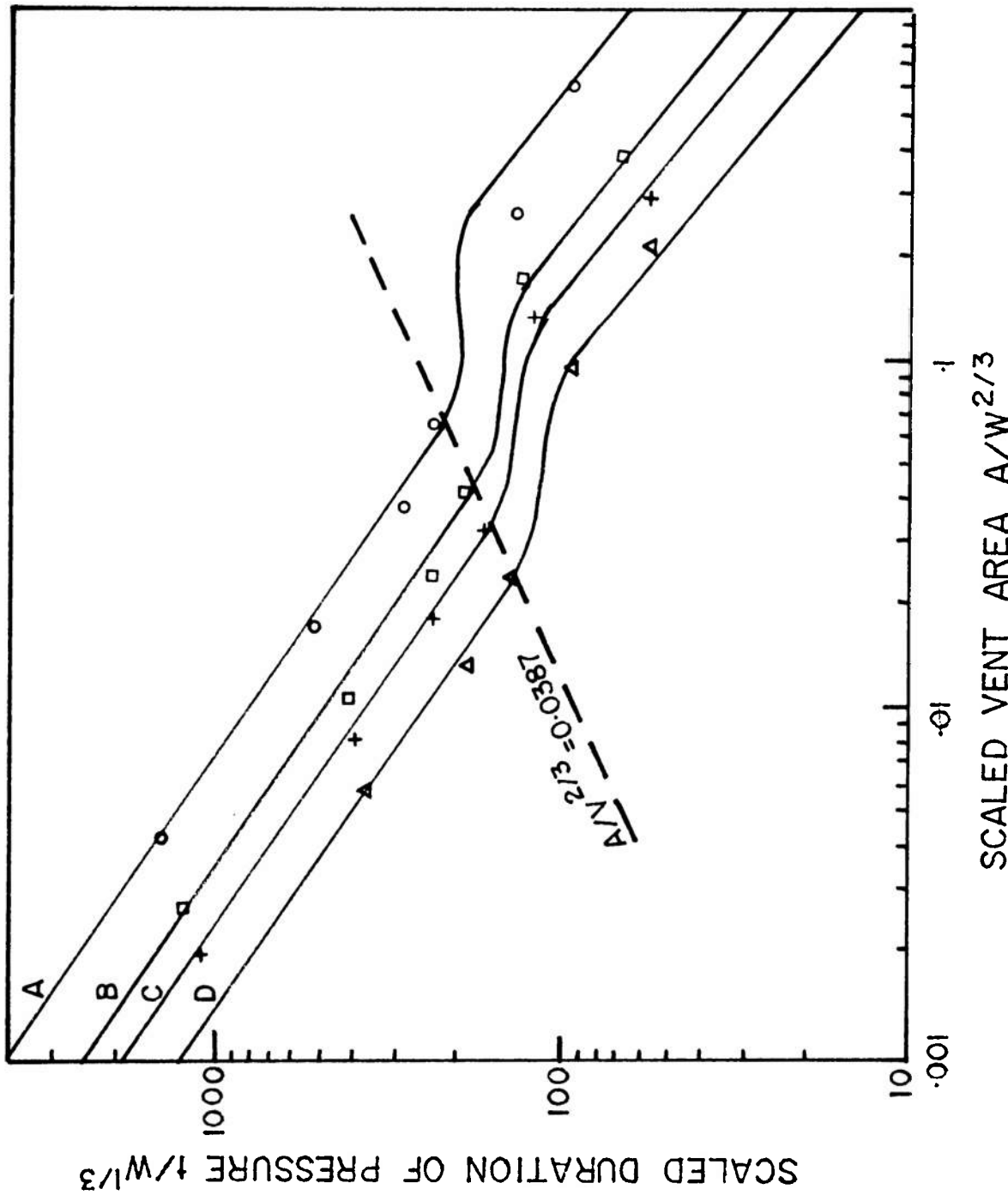
The scaled duration of positive pressure ($t/W^{1/3}$) is shown as a function of the scaled vent area in figures 31 through 35. The curves consist of a family of straight lines, then another family of lines displaced vertically and of different slope from the first. The point at which the lines deviate from straight as vent size was increased is at the same value of $A/V^{2/3}$ as for the impulse curves (see line marked $A/V^{2/3}$ on graph).

The straight line portions of the curves follows the equation

$$t/W^{1/3} = a((A/W^{2/3}) (W/V))^b \quad (7)$$

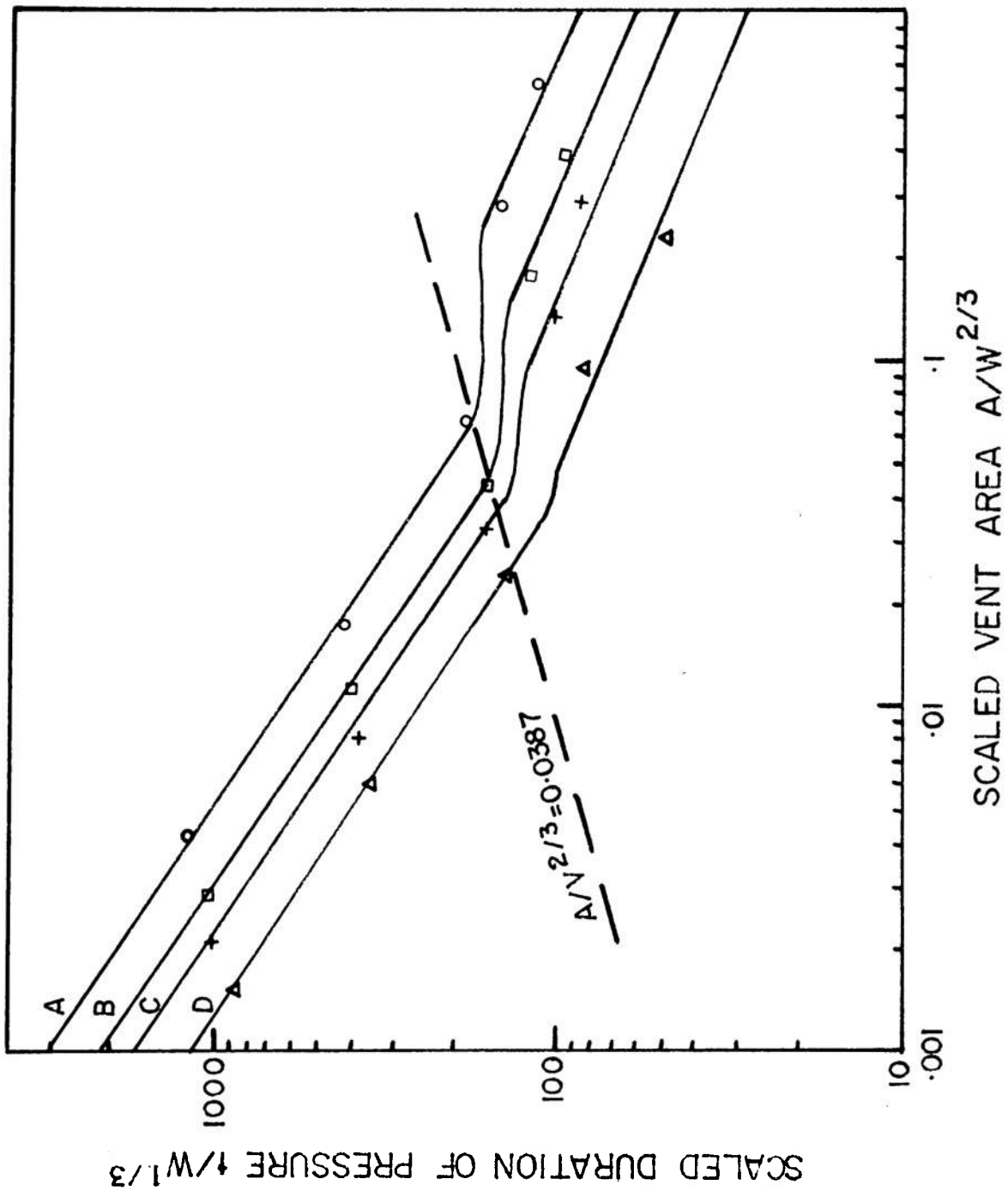
(table A-6). Only two points could be used to draw some of the lines; however, the shape appears to be similar to that of ref 1, so the lines were drawn accordingly.

As extension of the lines for larger vents indicate that the duration for smaller vents was less than would be expected from



Note: Curves represent the following loading densities: $a = 0.416$, $b = 0.830$, $c = 1.25$, $d = 2.08$.

Figure 31. Graphs of scaled duration of pressure versus scaled vent area for SI-193



Note: Curves represent the following loading densities: $a = 0.416$, $b = 0.830$, $c = 1.25$, $d = 2.08$.

Figure 32. Graphs of scaled duration of pressure versus scaled vent area for FW-306

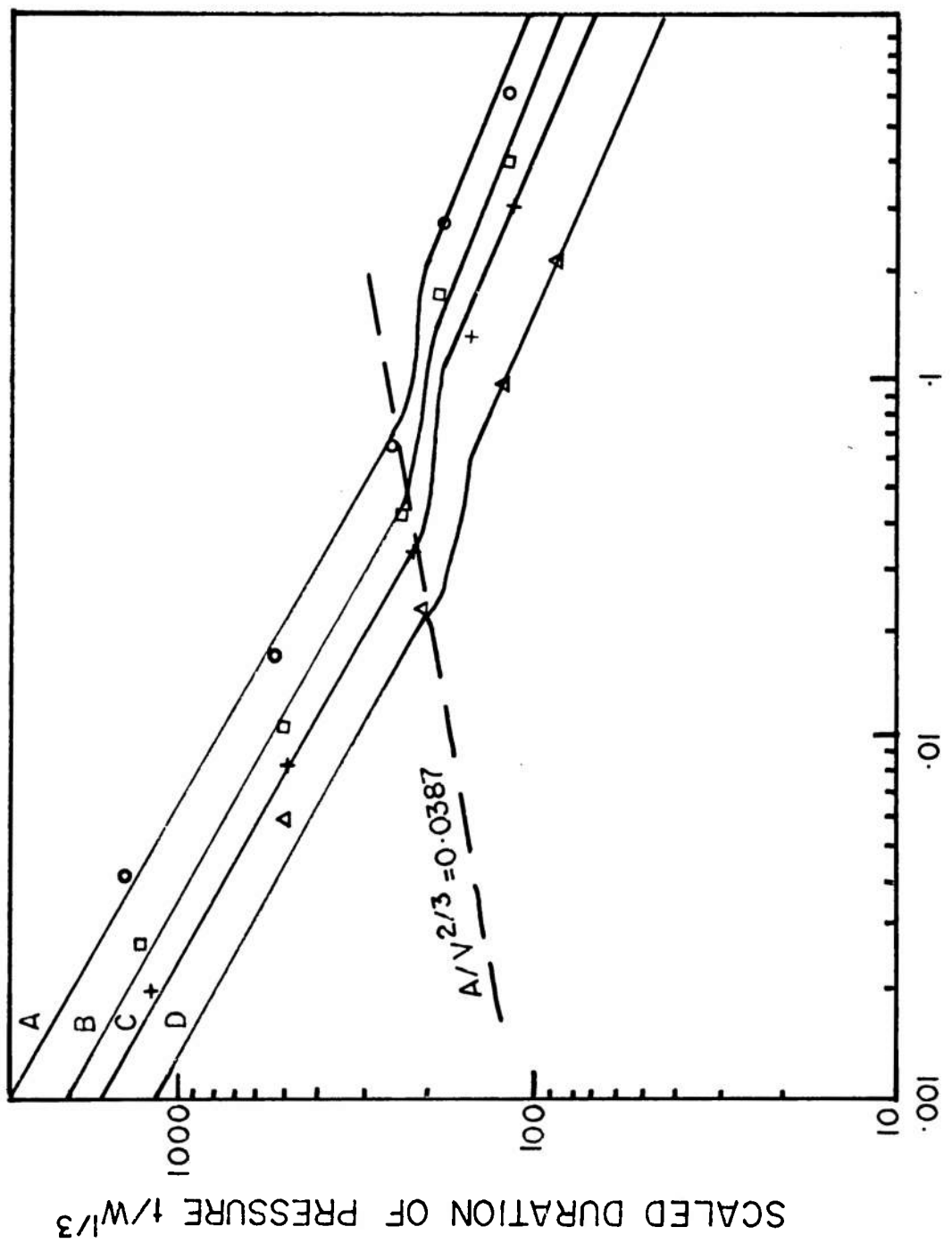


Figure 33. Graphs of scaled duration of pressure versus scaled vent area for PFP-555

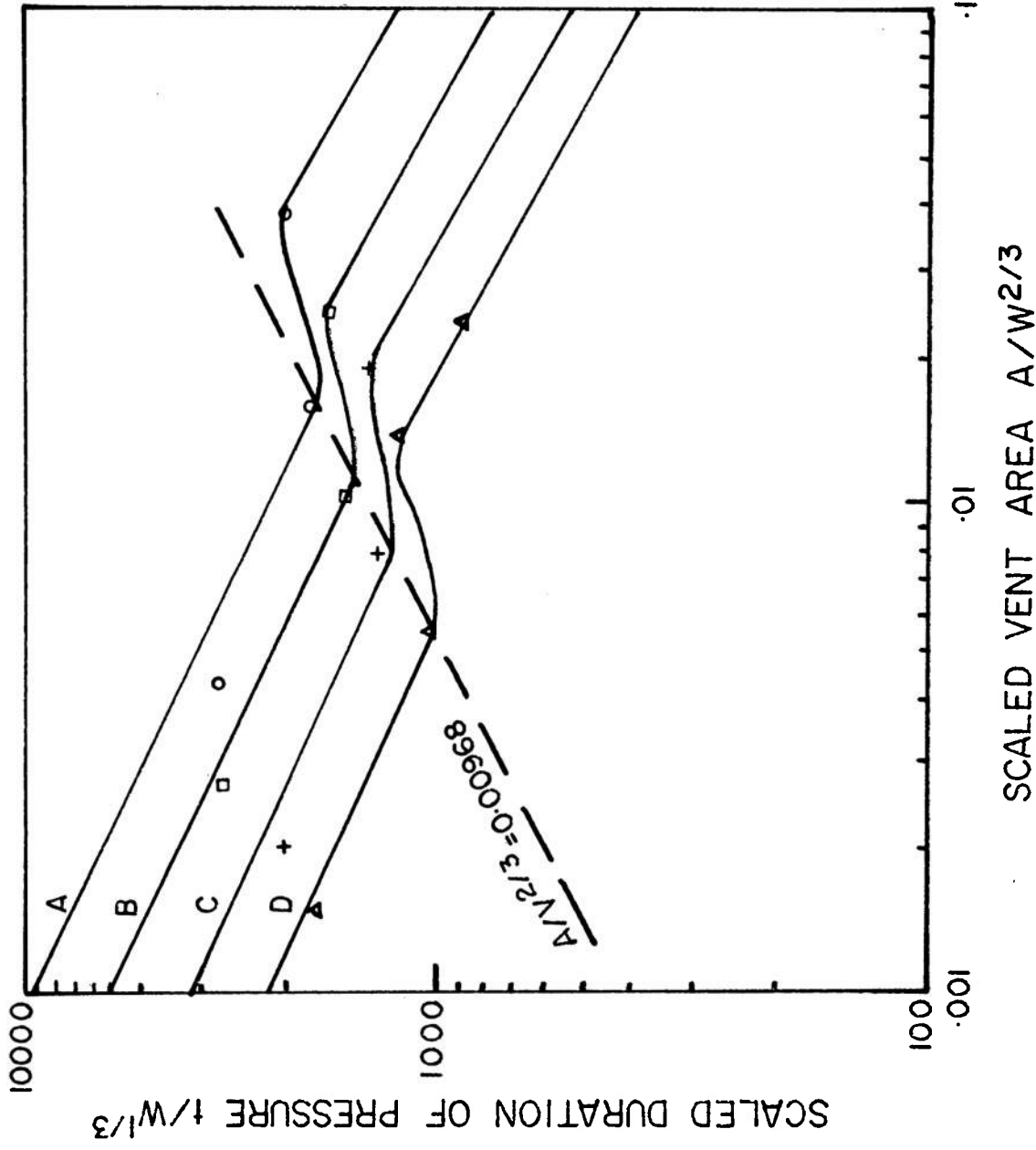
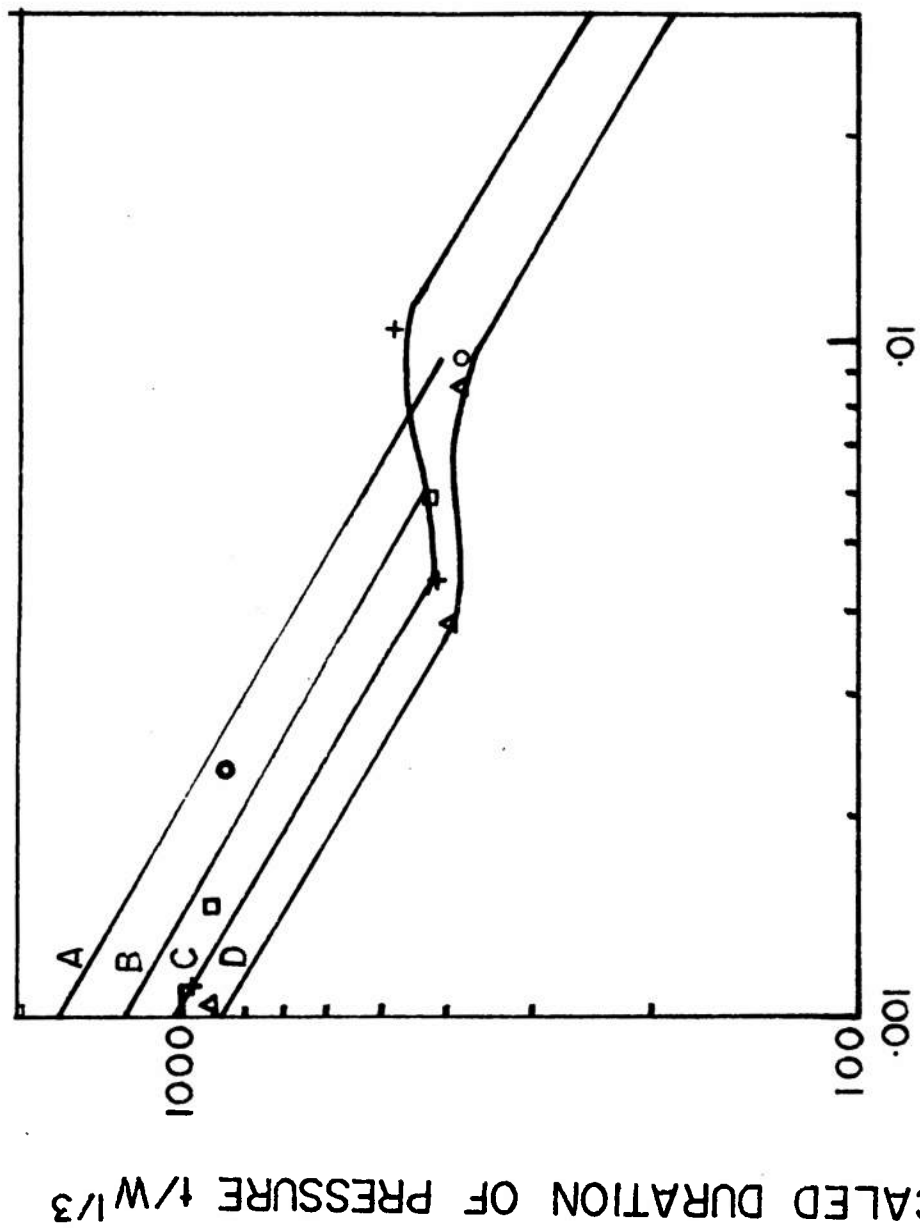


Figure 34. Graphs of scaled duration of pressure versus scaled vent area for FY-1451



SCALED VENT AREA $A/W^{2/3}$
 Note: Curves represent the following loading densities:
 $a = 1.04$,
 $b = 2.08$, $c = 3.12$, $d = 4.16$.

Figure 35. Graphs of scaled duration of pressure versus scaled vent area for DP-973.

simple confinement of the gaseous products. This fact bears out the contention that the burning process changed with confinement, with attendant acceleration of the combustion process.

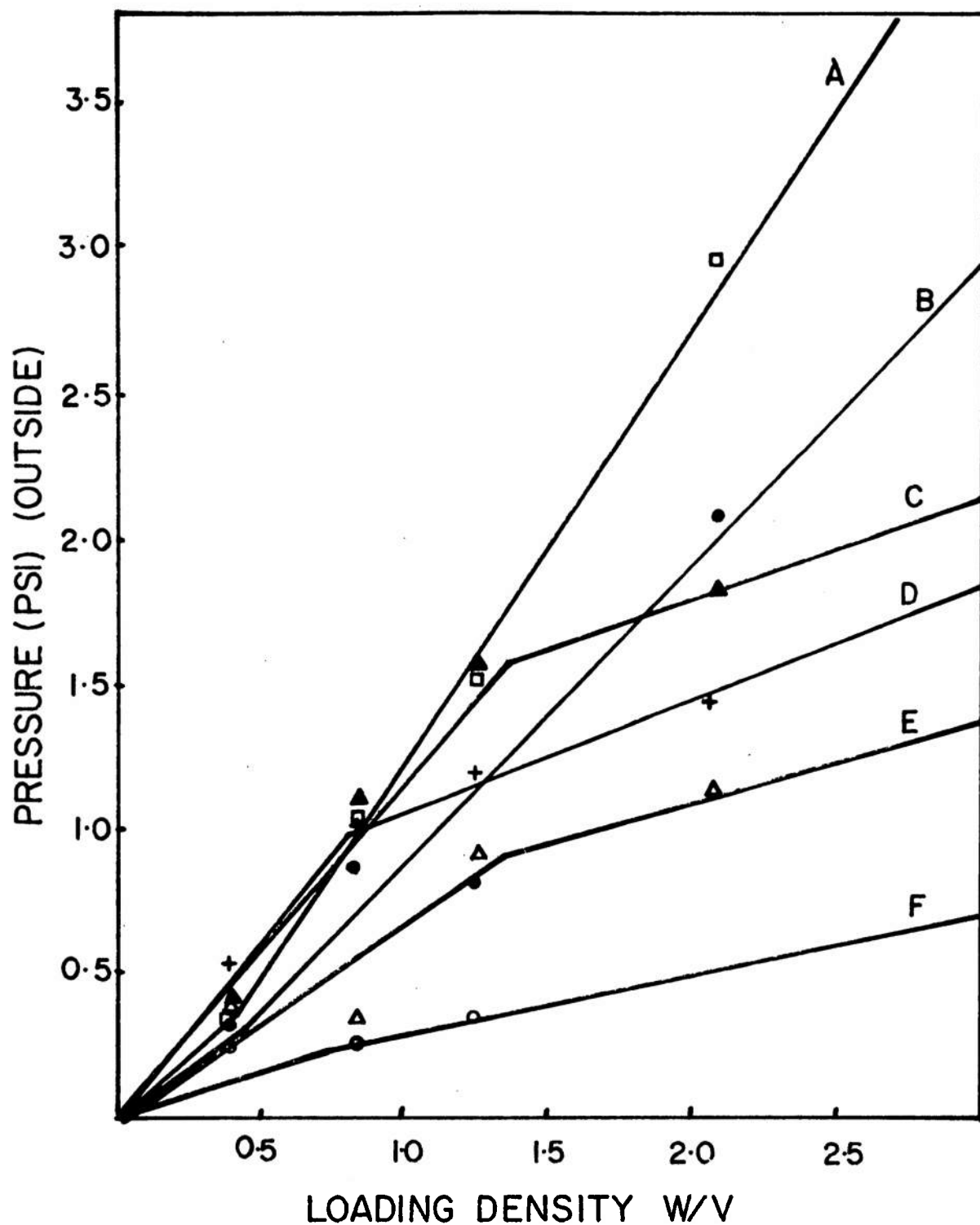
For larger vents, PFP-555 had a longer duration than SI-193 or FW-306. This would result in the observed lower peak pressures, as more gas could leak out during the burning. The duration for FY-1451 was, as expected, much longer than for any of the above three compositions. However, DP-973 had a scaled duration comparable to the fast burning compositions. Since this was a relatively gasless composition, not much pressure could build up even in a closed system, so that even with a short duration, low pressures were reached.

Pressure Environment Outside the Vessel

The pressure environment outside the vessel was much less clear and much less reproducible than that inside the vessel. Several detectors were used, one at 40 cm (16 in.) from the lid of the vessel, and one at 71 cm (28 in.). A third detector at 117 cm (46 in.) in the initial experiments but placed 366 cm (12 feet) from the vent and facing it in the later ones. The maximum pressure obtained was not registered on the same gauge for duplicate runs; sometimes the middle one was higher and sometimes either end. The only way to treat the data was to plot the maximum pressure obtained from any gauge as peak pressure; this was done in figures 36 through 39. There was a pressure rise as W/V was increased, but the pressure generally fell off as vent size was narrowed. This would be due to a slower leakage of gaseous products from the vessel with small vents, giving a smaller pressure peak outside. The duration of pressure was very difficult to measure since it was so short. There was also a great deal of rapid oscillatory behavior exhibited, making the actual duration of positive pressure uncertain.

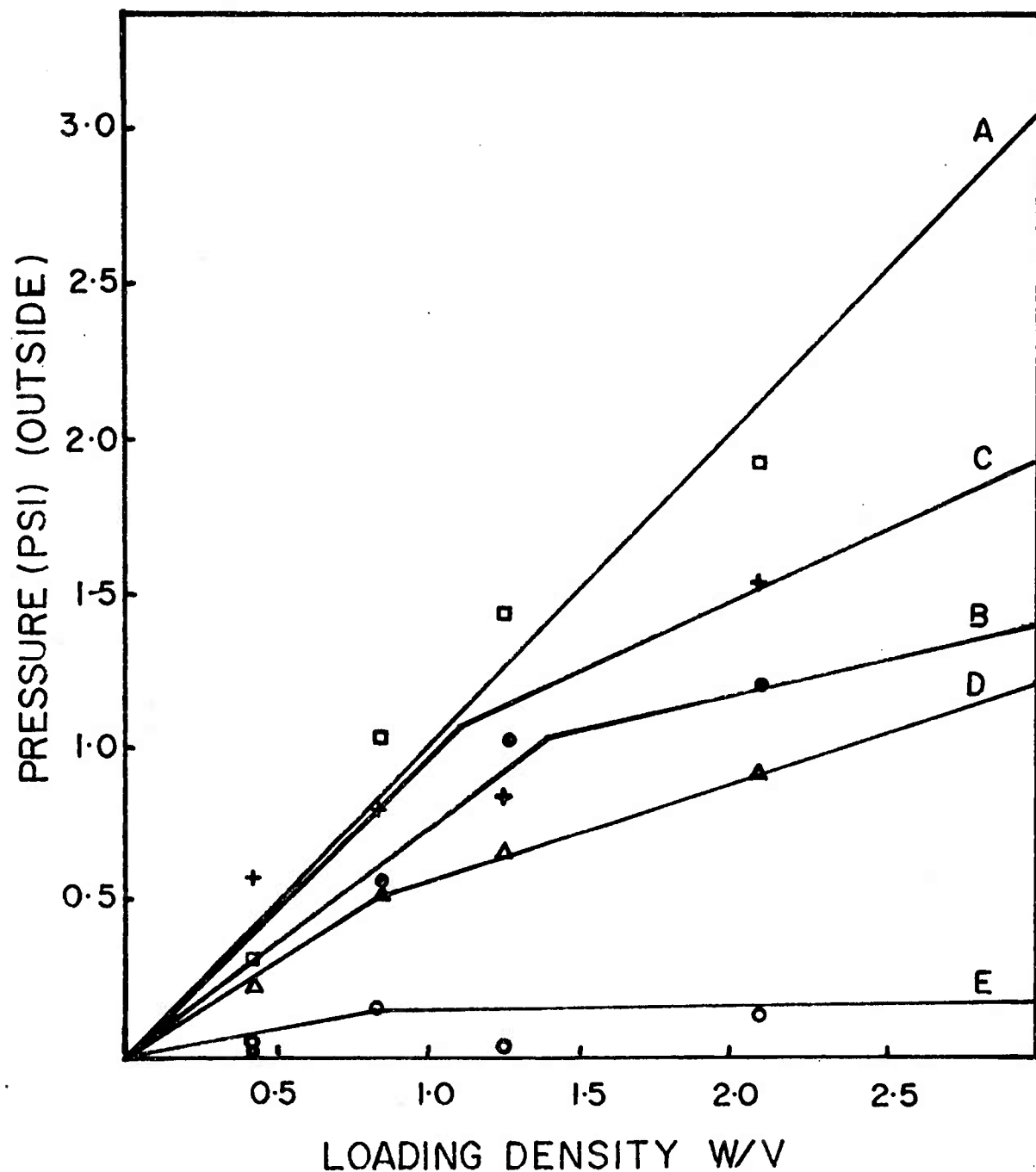
The pressure outside generally exhibited the same trends seen inside the vessel, that is, SI-193 was the greatest, followed by FW-306 and PFP-555. Pressure from FY-1451 was very low for small weights due to slow buildup and resultant low pressure head. For DP-973, pressure outside was nonexistent; the pressure head was too small and the vent also was too small.

An unusual result occurred with these detectors. A large (~ 7 PSI) negative pressure appeared, peaking as long as 30 seconds after the ignition. It is thought that this was not a real pressure, but a buildup of charge on the detector from the ions produced in the burning. The case of the detector was grounded but the charge must travel from the detector surface to the case. By ungrounding the



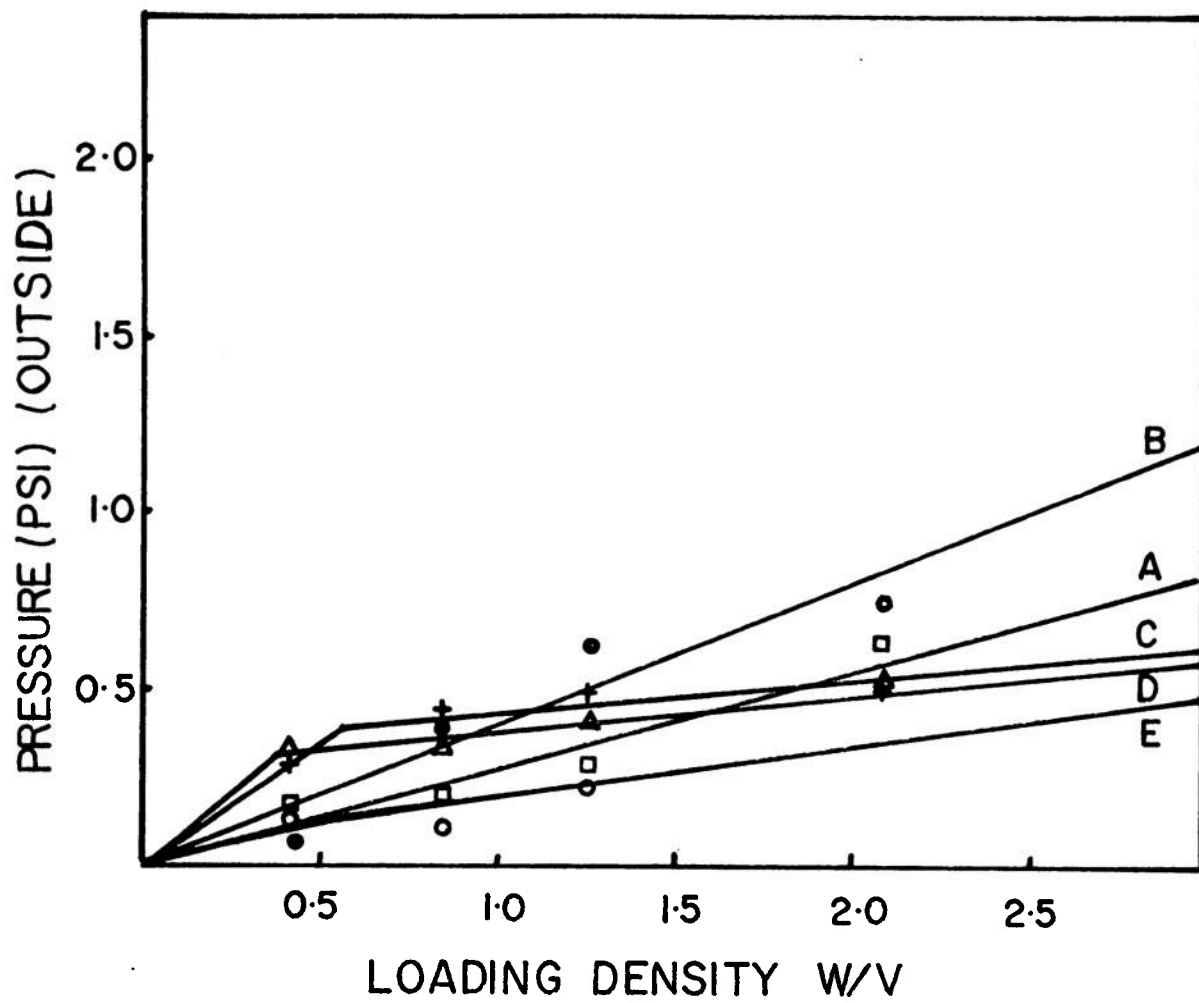
Note: Curves represent the following venting: a = 3 in., b = 2 in., c = 1 in., d = 3/4 in., e = 1/2 in., f = 1/4 in.

Figure 36. Graphs of pressure outside vessel versus loading density for SI-193



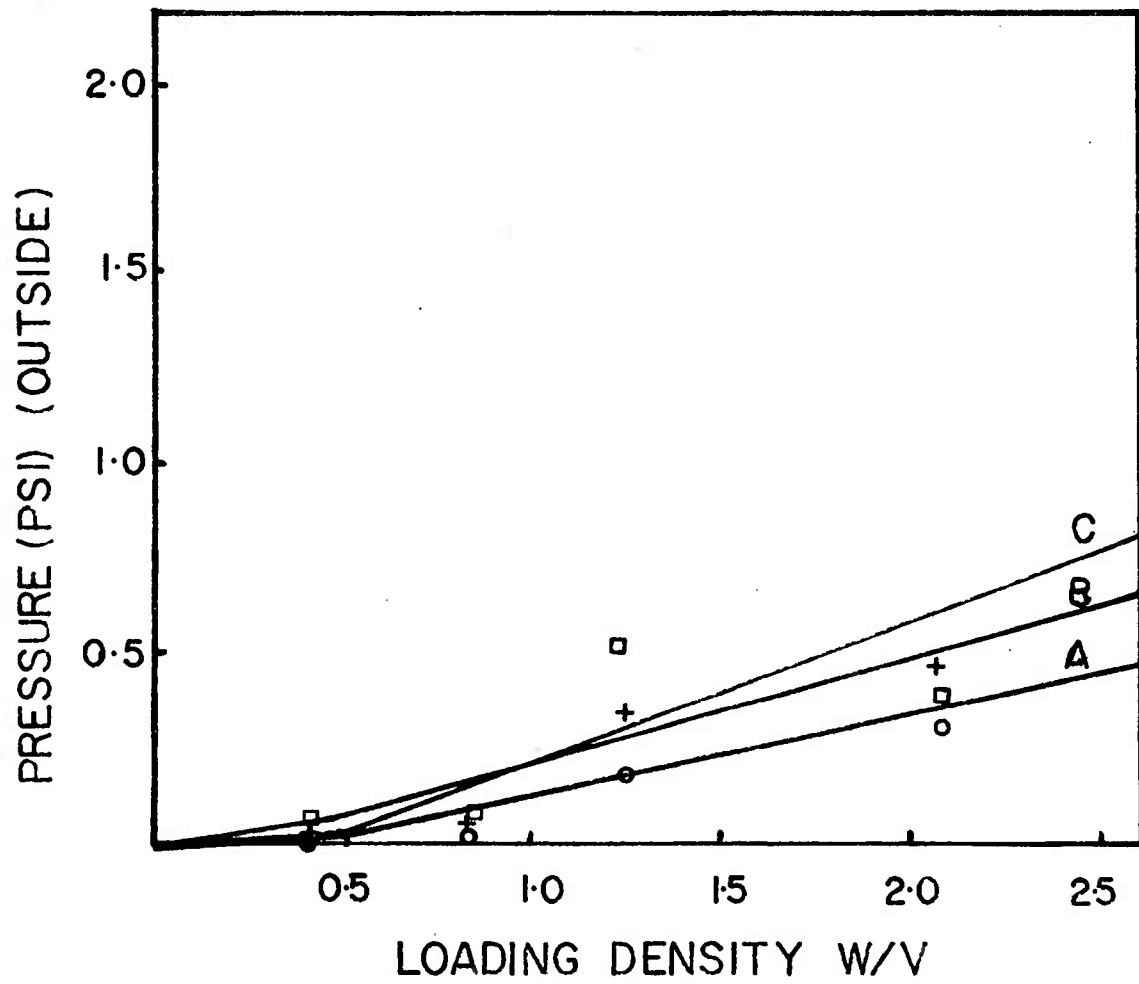
Note: Curves represent the following venting: a = 3 in., b = 2 in.,
 c = 1 in., d = 1/2 in., e = 1/4 in.

Figure 37. Graphs of pressure outside vessel versus loading density for FW-306



Note: Curves represent the following venting: a = 3 in., b = 2 in., c = 1 in., d = 1/2 in., e = 1/4 in.

Figure 38. Graphs of pressure outside vessel versus loading density for PFP-555



Note: Curves represent the following venting: a = 3/4 in., b = 1/2 in., c = 1/4 in.

Figure 39. Graphs of pressure outside vessel versus loading density for FY-1451

case, it was possible to lengthen the time required for the signal to return to zero to several minutes, confirming the above explanation.

The detector, 366 cm (12 feet) from the vessel, was used primarily to measure the velocity of the pressure wave. Any difference less than 12 milliseconds in the onset of pressure between detectors 1 and 5 would be supersonic. Velocities in excess of 330 m/sec (speed of sound) were obtained in several cases, mostly for FW-306. However, the velocity measured was a minimum value, since many of the traces for detector 1 had a small tail at the beginning, lengthening the apparent time different between detectors 1 and 5. Table 3 lists the number of samples which definitely produced this supersonic wave; it also lists the ones that possibly would produce it if the tail were not there, and it lists the number of samples measured for each composition. It is of interest that all of the samples mentioned definitely producing a supersonic wave, and all but a few of the possible ones, produced data in the high output group mentioned earlier.

Table 3. Compositions with supersonic pressure wave

	<u>SI-193</u>	<u>PFP-555</u>	<u>FW-306</u>	<u>FY-1451</u>	<u>TOTAL</u>
Definite	2	0	14	0	16
Possible	<u>40</u>	<u>16</u>	<u>24</u>	<u>3</u>	<u>83</u>
Total	42	16	38	3	99
Total measured:					
	62	32	54	9	157

One definition of a detonation is a reaction producing a supersonic pressure wave. Using this definition, there have been low velocity detonations produced by these thermally ignited compositions; however, the velocity is only mach 1.4, compared to mach 10 or more for secondary explosives.

TNT Equivalencies

A calibration for TNT equivalency was obtained by igniting C₄, with a detonator, in the vessel. Two, four, and six grams of C₄ were detonated with a 7.6 cm (3 in.) vent on the vessel and gave a linear response of pressure versus W/V. Two grams were chosen as the calibration weight because it was less likely to damage the system. There did not appear to be much change in peak pressure from 2.5 to 1.3 cm (2 to 1 in.) vents so no vent smaller than 1.3 cm was tried.

The values obtained for this system matched well the data in ref 1; therefore, values for impulse with vents less than 1.3 cm were taken from the graphs presented therein.

The largest value for pressure equivalency obtained is 0.16 for SI-193 with a 0.6 cm (1/4 in.) vent. The values tended to be about the same for different weights with a given vent, so average values are reported in table 4. The values for DP-973 were so small as to be considered zero; this gasless composition just didn't produce much pressure.

Table 4. TNT equivalencies for pressure

Vent		SI-193	PFP-555	FW-306	FY-1451	DP-973
cm	(in.)					
7.6	3	.014	.0039	.013	-	-
5.0	2	.021	.0069	.015	-	-
2.5	1	.057	.024	.045	.0025	-
1.9	3/4	.094	-	-	.0057	2.6×10^{-5}
1.3	1/2	.11	.054	.077	.017	.0038
0.6	1/4	.16	.13	.11	.064	.0060

Values as high as 0.9 were obtained for impulse equivalencies as reported in table 5. Even DP-973 had an equivalency of 0.05 for impulse. This is due to the much longer duration, although at a lower pressure, exhibited by these compositions. Whereas the maximum dP/dt for the pyrotechnic composition was 108,000, the values for C4 were 360,000 to 600,000, while scaled durations of pressure for C4 were about 10 to 20% of the composition durations, and considerably less for the blast wave. This demonstrates the rapidity of combustion for the explosive materials but also the damage potential of the pyrotechnics due to their lengthy application of the force.

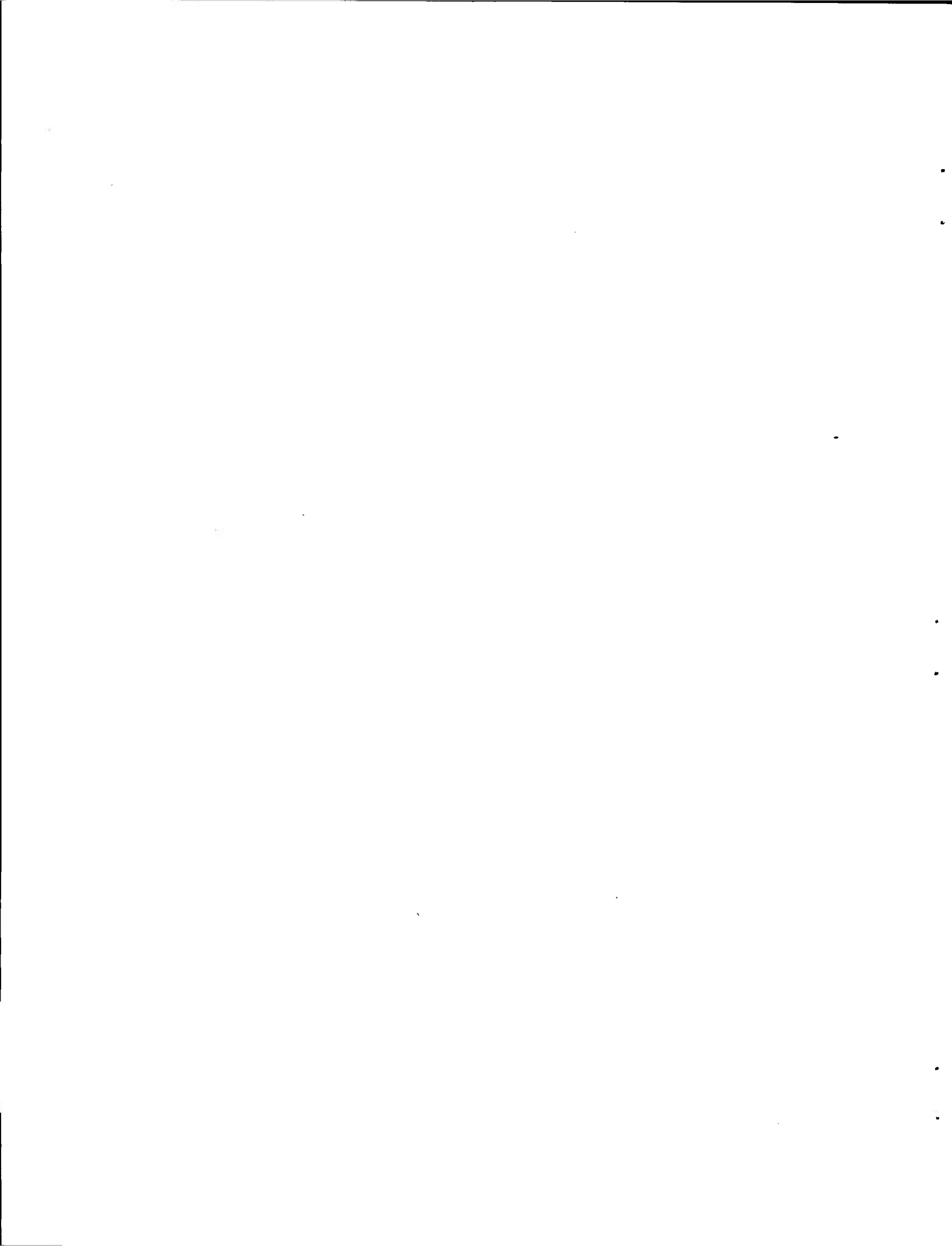
Table 5. TNT equivalencies for impulse

cm	(in.)	SI-193	PFP-555	FW-306	FY-1451	DP-973
7.6 cm	3	.13	.065	.18	-	-
5.0	2	.20	.14	.18	-	-
2.5	1	.30	.19	.23	.073	-
1.9	3/4	.52	-	-	.22	.0010
1.3	1/2	.54	.44	.44	.44	.032
0.6	1/4	.71	.59	.61	.87	.049

CONCLUSIONS

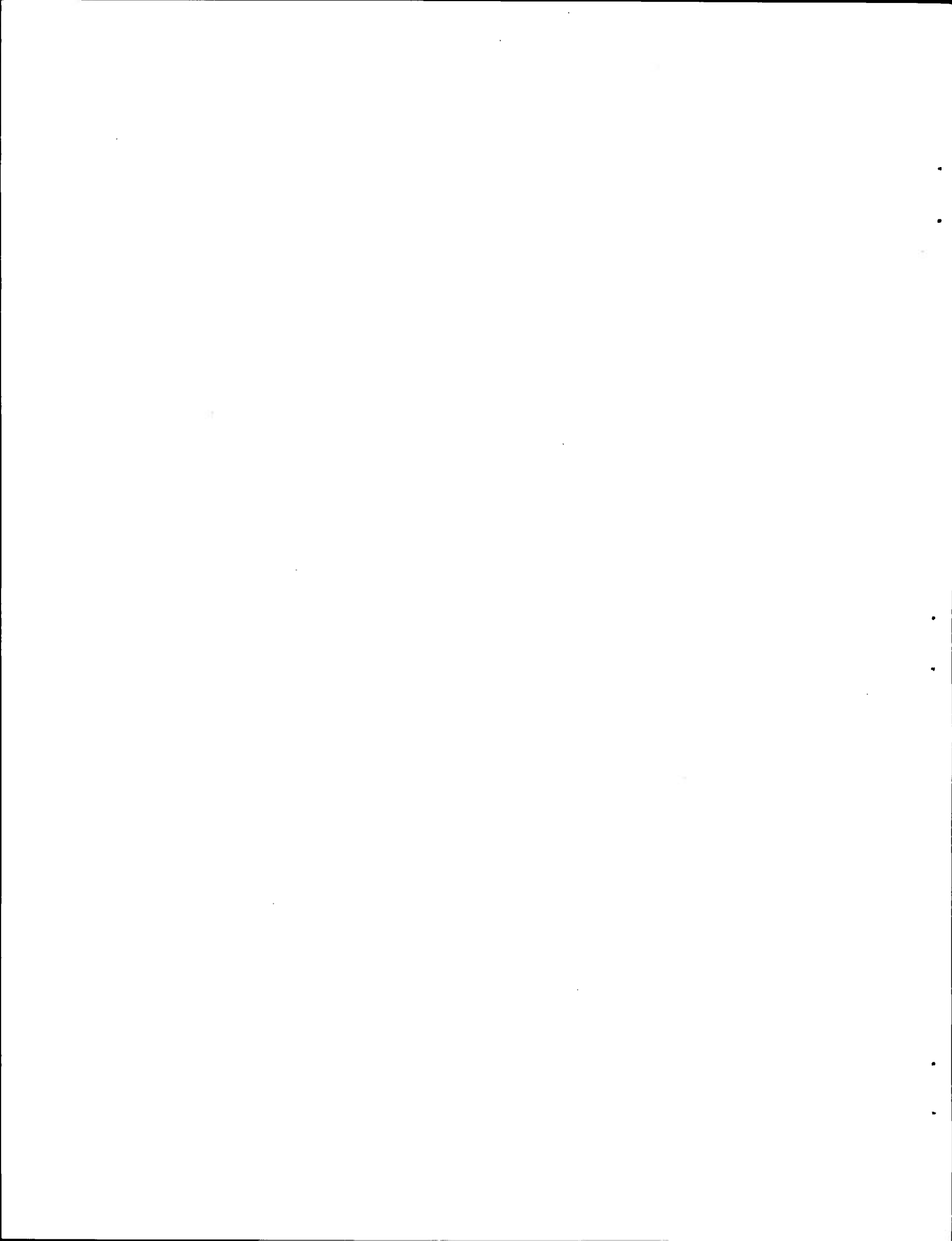
The results of the tests described in the report indicate that pyrotechnic compositions are indeed hazardous and that new criteria are required to judge their hazardous nature, rather than attempting to apply nonapplicable ones used for explosives. For example, explosives reach a high pressure very quickly resulting in a large blast wave, but the extremely short duration yields a relatively small impulse imparted to contingent walls of a room. The blast wave also tends to be more directional. This is more likely to punch a hole in a wall or break it into small pieces, as from a hammer blow. In addition, a large pressure from the blast wave is relayed outside the room, if one wall is left open. Pyrotechnics, on the other hand, produce lower pressure but last longer, giving a large impulse to the whole wall which can push the wall down. Little pressure is relayed outside since the buildup is slow and there is little or no blast wave. Thus, adjacent buildings would be less endangered from the blast wave, at a closer distance, than from an explosive. However, the extreme heat developed by some burning pyrotechnics can be of greater danger than the pressure; for instance FW-306 did not develop sufficient pressure to shear the bolts holding the lid, but the heat from the reaction melted the top of the stainless steel vessel. With proper venting, pressures from the combustion of pyrotechnics could be held to small values; but the heat and flame generated could harm people in the area, could set fires, or could even ignite other compositions located nearby.

Finally, it is possible, with sufficient confinement producing a large pressure buildup, to cause the burning of some of the pyrotechnics to become a low velocity detonation at which point explosives criteria would apply. One should bear in mind, however, the extremely hazardous nature of pyrotechnic deflagrations, and the need to develop appropriate criteria for describing their outputs.



REFERENCES

1. W.A. Keenan and J.E. Tancreto, "Blast Environment from Fully and Partially Vented Explosive in Cubicles," Sixteenth Annual Explosive Safety Seminar, Hollywood, FL, September 1974.
2. G.F. Kinney and R.C.S. Sewell, Venting of Explosives, NWC Technical Memorandum 2448, Naval Weapons Center, China Lake, CA, July 1974.
3. H.S. Napadensky, J.J. Swatosh, Jr., and A. Humphreys, "TNT Equivalency of Three Pyrotechnic Compositions," Technical Report 4628, Picatinny Arsenal, (now ARRADCOM), Dover, NJ, June 1974.
4. G.J. Petino and F. Taylor, "Propagation and/or Detonation Tests of Pyrotechnic Compositions," Technical Report 2146, Picatinny Arsenal, Dover, NJ, July 1974.
5. R. Collett, "Propagation Rates in Thermally Ignited Pyrotechnic Compositions," Technical Report ARLCD-TR-77049, ARRADCOM, Dover, NJ, August 1978.
6. S. Resnick, "Simulated High Altitude Tests of Illuminating Compositions," Technical Report 2166, Picatinny Arsenal, Dover, NJ, April 1955.
7. P. Farnell, unpublished work, 1972.



APPENDIX
LIST OF EQUATIONS WITH CONSTANTS

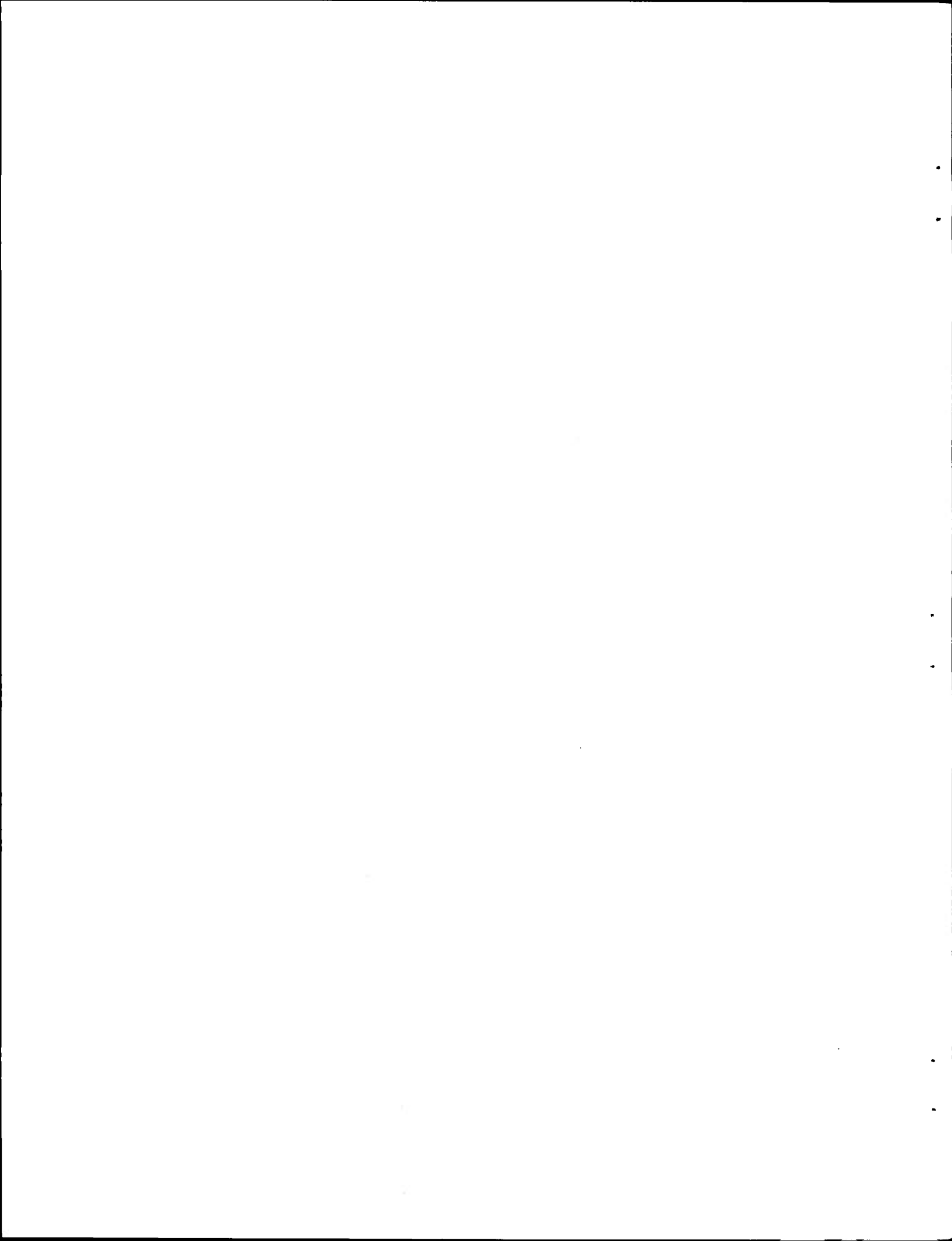


Table A-1. Equations for pressure versus loading density

SI-193	7.6 cm Vent 5.0 cm Vent 2.5 cm Vent 1.9 cm Vent 1.3 cm Vent 0.6 cm Vent	P = 90 W/V - 70 P = 81 W/V - 13 P = 197 W/V + 19 P = 343 W/V P = 397 W/V P = 430 W/V + 105
PFP-555	7.6 cm Vent 5.0 cm Vent 2.5 cm Vent 1.3 cm Vent 0.6 cm Vent	P = 22 W/V - 16 P = 80 W/V - 64 P = 95.5 W/V P = 197 W/V P = 320 W/V
FW-306	7.6 cm Vent 5.0 cm Vent 2.5 cm Vent 1.3 cm Vent 0.6 cm Vent	P = 45 W/V - 17 P = 76 W/V - 27 P = 174 W/V P = 234 W/V + 46 P = 190 W/V + 163
FY-1451	1.9 cm Vent 1.3 cm Vent 0.6 cm Vent	P = 75 W/V - 60 P = 170 W/V - 110 P = 500 W/V - 275
DP-973	1.3 cm Vent 0.6 cm Vent	P = 7.75 W/V + 8.5 P = 14.5 W/V + 13

Table A-2. Equations for pressure versus vent

SI-193	10 g	$P = -210 \ln (A/V^{2/3}) - 188$
	20 g	$P = -135 \ln (A/V^{2/3}) - 137$
	30 g	$P = -95.1 \ln (A/V^{2/3}) - 106$
	50 g	$P = -73.3 \ln (A/V^{2/3}) - 162$
PFP-555	10 g	$P = -45.5 \ln (A/V^{2/3}) - 121$
	20 g	$P = -63.0 \ln (A/V^{2/3}) - 125$
	30 g	$P = -63.0 \ln (A/V^{2/3}) - 75$
	50 g	$P = -80.3 \ln (A/V^{2/3}) - 55$
FW-306	10 g	$P = -59.6 \ln (A/V^{2/3}) - 130$
	20 g	$P = -72.5 \ln (A/V^{2/3}) - 99$
	30 g	$P = -83.8 \ln (A/V^{2/3}) - 75$
	50 g	$P = -122 \ln (A/V^{2/3}) - 81$
FY-1451	10 g	$P = -19.3 \ln (A/V^{2/3}) - 84$
	20 g	$P = -78.9 \ln (A/V^{2/3}) - 329$
	30 g	$P = -261 \ln (A/V^{2/3}) - 1130$
	50 g	$P = -292 \ln (A/V^{2/3}) - 1080$
DP-973	25 g	$P = -10.8 \ln (A/V^{2/3}) - 30$
	50 g	$P = -14.0 \ln (A/V^{2/3}) - 38$
	75 g	$P = -30.0 \ln (A/V^{2/3}) - 116$
	100 g	$P = -31.7 \ln (A/V^{2/3}) - 114$

Table A-3. Equations for dP/dt versus loading density

SI-193	7.6 cm Vent 5.0 cm Vent 2.5 cm Vent 1.9 cm Vent 1.3 cm Vent 0.6 cm Vent	$dP/dt = 8750 \text{ W/V} - 5750$ $dP/dt = 11800 \text{ W/V} - 6600$ $dP/dt = 14800 \text{ W/V}$ $dP/dt = 35300 \text{ W/V} = 4600$ $dP/dt = 43700 \text{ W/V} - 5400$ $dP/dt = 52200 \text{ W/V}$
PFP-555	7.6 cm Vent 5.0 cm Vent 2.5 cm Vent 1.3 cm Vent 0.6 cm Vent	$dP/dt = 2650 \text{ W/V} - 2000$ $dP/dt = 5550 \text{ W/V} - 3800$ $dP/dt = 6800 \text{ W/V} - 1400$ $dP/dt = 9500 \text{ W/V}$ $dP/dt = 14800 \text{ W/V}$
FW-306	7.6 cm Vent 5.0 cm Vent 2.5 cm Vent 1.3 cm Vent 0.6 cm Vent	$dP/dt = 2100 \text{ W/V}$ $dP/dt = 9000 \text{ W/V} - 5000$ $dP/dt = 24600 \text{ W/V} - 7000$ $dP/dt = 27600 \text{ W/V}$ $dP/dt = 37000 \text{ W/V}$
FY-1451	1.9 cm Vent 1.3 cm Vent 0.6 cm Vent	$dP/dt = 1000 \text{ W/V} = 1100$ $dP/dt = 3630 \text{ W/V} - 3950$ $dP/dt = 4660 \text{ W/V} - 3220$
DP-973	1.3 cm Vent 0.6 cm Vent	$dP/dt = 210 \text{ W/V} + 310$ $dP/dt = 200 \text{ W/V} + 750$

Table A-4. Equations for dP/dt versus vent

SI-193	10 g	$dP/dt = -4910 \ln (A/V^{2/3}) - 8340$
	20 g	$dP/dt = -9160 \ln (A/V^{2/3}) - 14300$
	30 g	$dP/dt = -14800 \ln (A/V^{2/3}) - 21200$
	50 g	$dP/dt = -21600 \ln (A/V^{2/3}) - 18800$
PPF-555	10 g	$dP/dt = -1860 \ln (A/V^{2/3}) - 4470$
	20 g	$dP/dt = -2300 \ln (A/V^{2/3}) - 2800$
	30 g	$dP/dt = -4170 \ln (A/V^{2/3}) - 6520$
	50 g	$dP/dt = -3910 \ln (A/V^{2/3}) - 175$
FW-306	10 g	$dP/dt = -1690 \ln (A/V^{2/3}) - 1990$
	20 g	$dP/dt = -8730 \ln (A/V^{2/3}) - 15200$
	30 g	$dP/dt = -10600 \ln (A/V^{2/3}) - 10400$
	50 g	$dP/dt = -14200 \ln (A/V^{2/3}) - 11000$
FY-1451	10 g	$dP/dt = -62.1 \ln (A/V^{2/3}) - 236$
	20 g	$dP/dt = -236 \ln (A/V^{2/3}) - 868$
	30 g	$dP/dt = -1960 \ln (A/V^{2/3}) - 8540$
	50 g	$dP/dt = -2170 \ln (A/V^{2/3}) - 7000$
DP-973	25 g	$dP/dt = -329 \ln (A/V^{2/3}) - 997$
	50 g	$dP/dt = -345 \ln (A/V^{2/3}) - 900$
	75 g	$dP/dt = -298 \ln (A/V^{2/3}) - 544$
	100 g	$dP/dt = -491 \ln (A/V^{2/3}) - 1150$

Table A-5. Equations for scaled impulse versus scaled vent area

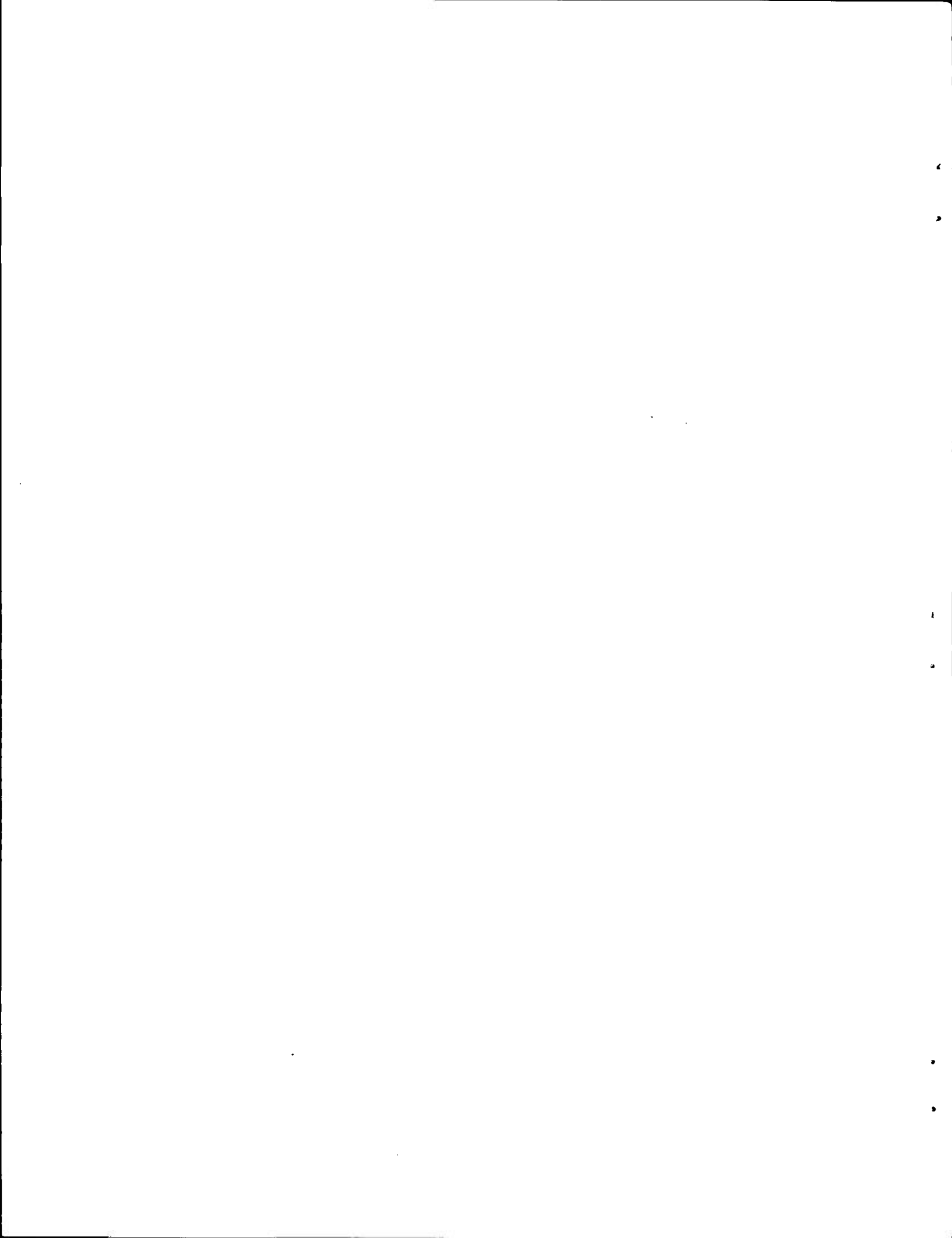
<u>Composition</u>	<u>Equation</u>	<u>Applicable weight (g)</u>
SI-193	$i/W^{1/3} = 517 (A/W^{2/3})^{-0.969}$	A11
PFP-555	$i/W^{1/3} = 609 (A/W^{2/3})^{-0.998}$	20, 30, 50
	$i/W^{1/3} = 206 (A/W^{2/3})^{-1.06}$	10
FW-306	$i/W^{1/3} = 829 (A/W^{2/3})^{-0.824}$	A11
FY-1451	$i/W^{1/3} = 145 (A/W^{2/3})^{-1.17} (W/V)^{0.5}$	A11
DP-973	$i/W^{1/3} = 13.7 (A/W^{2/3})^{-1.11}$	A11

Table A-6. Equations for scaled duration of positive pressure versus scaled vent area

<u>Composition</u>	<u>Equation</u>	<u>Applicable A/V^{2/3}</u>
SI-193	$t/W^{1/3} = 18.3 \{(A/W^{2/3}) (W/V)\}^{-0.694}$	<0.0387
	$t/W^{1/3} = 29.3 \{(A/W^{2/3}) (W/V)\}^{-0.807}$	>0.155
PFP-555	$t/W^{1/3} = 35 \{(A/W^{2/3}) (W/V)\}^{-0.57}$	<0.0387
	$t/W^{1/3} = 76 \{(A/W^{2/3}) (W/V)\}^{-0.446}$	>0.155
FW-306	$t/W^{1/3} = 15.5 \{(A/W^{2/3}) (W/V)\}^{-0.685}$	<0.0387
	$t/W^{1/3} = 58 \{(A/W^{2/3}) (W/V)\}^{-0.445}$	>0.155
FY-1451	$t/W^{1/3} = 122 \{(A/W^{2/3}) (W/V)\}^{-0.5}$	<0.00968
	$t/W^{1/3} = 186 \{(A/W^{2/3}) (W/V)\}^{-0.58}$	>0.0278
DP-973	$t/W^{1/3} = 31 \{(A/W^{2/3}) (W/V)\}^{-0.59}$	<0.00968

List of Symbols

V	= volume of vessel (ft ³)
A	= area of vent (ft ²)
P	= pressure (PSI)
t	= time (sec)
dP/dt	= rate of pressure rise
p	= peak pressure observed from trace (PSI)
W/V	= loading density of charge in vessel
W	= weight of composition (lbs)
A/V ^{2/3}	= defines venting
i	= impulse (integral of pressure versus time trace) (PSI-msec)
i/W ^{1/3}	= scaled impulse
A/W ^{2/3}	= scaled vent area
t/w ^{1/3}	= scaled duration of positive pressure
AW ^{1/3} /V	= scaled degree of venting (A/W ^{2/3} .W)
P _o	= pressure outside vessel (PSI)
R	= distance from vessel to detectors outside (ft)



DISTRIBUTION LIST

Commander
U.S. Army Armament Research and
Development Command

ATTN: DRDAR-GCL
DRDAR-LCE, Dr. Walker (3)
Mr. L. Avrami
Mr. L. Frey
Mr. G. Jackman

DRDAR-LCE-T, Mrs. P. Farnell (10)
DRDAR-LCU, Mr. A.S. Roseff
Mr. A. Moss

DRDAR-SCA
DRDAR-TSS (5)

Dover, New Jersey 07801

Commander
U.S. Army Armament Materiel
Readiness Command

ATTN: DRSAR-LEP-L
Rock Island, IL 61299

Commander/Director
Chemical Systems Laboratory
U.S. Army Armament Research and
Development Command

ATTN: DRDAR-CLJ-L
DRDAR-CLB-PA
APG, Edgewood Area, MD 21010

Director
U.S. Army Materiel Systems Analysis
Activity
ATTN: DRXSY-MP
Aberdeen Proving Ground, MD 21005

Director
Ballistics Research Laboratory
U.S. Army Armament Research and
Development Command
ATTN: DRDAR-TSB-S
Aberdeen Proving Ground, MD 21005

Chief
Benet Weapons Laboratory, LCWSL
U.S. Army Armament Research and
Development Command
ATTN: DRDAR-LCB-TL
Watervliet, NY 12198

Director
U.S. Army TRADOC Systems
Analysis Activity
ATTN: ATAA-SL
White Sands Missile Range, NM 88002

Commander
Harry Diamond Laboratories
ATTN: Library, Room 211, Bldg. 92
Connecticut Ave & Van Ness St., N.W.
Washington, DC 20438

U.S. Army Research Office
ATTN: RDRD
P.O. Box 12211
Research Triangle Park, NC 27709

Commander
Naval Weapons Support Center
ATTN: Code 5042, Dr. B. Douda
Dr. H. Webster
Crane, IN 47522

Commander
Naval Weapons Center
ATTN: Code 3880, Dr. S. Reed
Code 233, Technical Library
China Lake, CA 93555

Commander
Naval Surface Weapons Center
White Oak Laboratory
ATTN: Code X-21, Tech Library
Silver Spring, MD 20910

Commander
Naval Air Systems Command
ATTN: Code AIR-310C, Dr. H. Rosenwasser
Code AIR-954, Technical Library
Washington, DC 20361

Commander
U.S. Naval Ordnance Station
ATTN: Scientific and Tech Info Div
Indian Head, MD 20640

Commander
Naval Sea Systems Command
ATTN: SEA-62R32, Mr. G. Edwards
SEA-09G3, Technical Library
Washington, DC 20362

Commander
Pacific Missile Test Center
Electro-Optics Division
ATTN: Technical Library
Pt. Mugu, CA 93042

Aeronautical Systems Division (AFSC)
ATTN: Technical Library
Wright-Patterson Air Force Base
Ohio 45433

Commander
U.S. Air Force
ATTN: AFATL/DLOSL
Eglin Air Force Base, FL 32542

Commander
Armament Development Test Center
ATTN: Code ADTC/SDWE
Eglin Air Force Base, FL 32542

Commander
Lowry Technical Training Center (TTOX)
Lowry AFB, CO 80230

Commander
Air Force Avionics Laboratory (AFSC)
ATTN: AFAL/WRW-3, Mr. F.E. Linton
Mr. R.D. Hunziker
AFAL-WRD-2, Mr. G.W. Schivley
Wright Patterson Air Force Base, OH 45433

NASA
Scientific & Technical Information
Facility
P.O. Box 33
College Park, MD 20740

Central Intelligence Agency
ATTN: CRS/ADD/Standard Distribution
Washington, DC 20505

U.S. Army Foreign Science and
Technology Center
ATTN: DRXST-CSI, Mr. J. Jacoby
220 Seventh St., NE
Charlottesville, VA 22901

Institute for Defense Analyses
ATTN: Library, Documents
400 Army-Navy Drive
Arlington, VA 22201

Administrator
Defense Technical Information Center
ATTN: Accessions Division (12)
Alexandria, VA 22314

Denver Research Institute
University of Denver
Denver, CO 80220

Battelle Memorial Institute
Columbus Laboratories
TACTEC
505 King Avenue
Columbus, OH 43201

